Model-independent determination of the strong-phase difference between D^0 and $\bar{D}^0 \to K^0_{S,L} h^+ h^-$ ($h = \pi, K$) and its impact on the measurement of the CKM angle γ/ϕ_3

J. Libby,[1] M. Kornicer,[2] R. E. Mitchell,[2] M. R. Shepherd,[2] C. M. Tarbert,[2] D. Besson,[3] T. K. Pedlar,[4] J. Xavier,[4] D. Cronin-Hennessy,[5] J. Hietala,[5] P. Zweber,[5] S. Dobbs,[6] Z. Metreveli,[6] K. K. Seth,[6] A. Tomaradze,[6] T. Xiao,[6] S. Brisbane,[7] S. Malde,[7] L. Martin,[7] A. Powell,[7] P. Spradlin,[7] G. Wilkinson,[7] H. Mendez,[8] J. Y. Ge,[9] D. H. Miller,[9] I. P. J. Shipsey,[9] B. Xin,[9] G. S. Adams,[10] D. Hu,[10] B. Moziak,[10] J. Napolitano,[10] K. M. Ecklund,[11] J. Insler,[12] H. Muramatsu,[12] C. S. Park,[12] L. J. Pearson,[12] E. H. Thorndike,[12] F. Yang,[12] S. Ricciardi,[13] C. Thomas,[7,13] M. Artuso,[14] S. Blusk,[14] N. Horwitz,[14] R. Mountain,[14] T. Skwarnicki,[14] S. Stone,[14] J. C. Wang,[14] L. M. Zhang,[14] T. Gershon,[15] G. Bonvicini,[16] D. Cinabro,[16] A. Lincoln,[16] M. J. Smith,[16] P. Zhou,[16] J. Zhu,[16] P. Naik,[17] J. Rademacker,[17] D. M. Asner,[18,*] K. W. Edwards,[18] K. Randrianarivony,[18] G. Tatishvili,[18,*] R. A. Briere,[19] H. Vogel,[19] P. U. E. Onyisi,[20] J. L. Rosner,[20] J. P. Alexander,[21] D. G. Cassel,[21] S. Das,[21] R. Ehrlich,[21] L. Fields,[21] L. Gibbons,[21] S. W. Gray,[21] D. L. Hartill,[21] B. K. Heltsley,[21] D. L. Kreinick,[21] V. E. Kuznetsov,[21] J. R. Patterson,[21] D. Peterson,[21] D. Riley,[21] A. Ryd,[21] A. J. Sadoff,[21] X. Shi,[21] W. M. Sun,[21] J. Yelton,[22] P. Rubin,[23] N. Lowrey,[24] S. Mehrabyan,[24] M. Selen,[24] and J. Wiss[24]

(CLEO Collaboration)

[1]*Indian Institute of Technology Madras, Chennai, Tamil Nadu 600036, India*
[2]*Indiana University, Bloomington, Indiana 47405, USA*
[3]*University of Kansas, Lawrence, Kansas 66045, USA*
[4]*Luther College, Decorah, Iowa 52101, USA*
[5]*University of Minnesota, Minneapolis, Minnesota 55455, USA*
[6]*Northwestern University, Evanston, Illinois 60208, USA*
[7]*University of Oxford, Oxford OX1 3RH, UK*
[8]*University of Puerto Rico, Mayaguez, Puerto Rico 00681*
[9]*Purdue University, West Lafayette, Indiana 47907, USA*
[10]*Rensselaer Polytechnic Institute, Troy, New York 12180, USA*
[11]*Rice University, Houston, Texas 77005, USA*
[12]*University of Rochester, Rochester, New York 14627, USA*
[13]*STFC Rutherford Appleton Laboratory, Chilton, Didcot, Oxfordshire, OX11 0QX, UK*
[14]*Syracuse University, Syracuse, New York 13244, USA*
[15]*University of Warwick, Coventry CV4 7AL, United Kingdom*
[16]*Wayne State University, Detroit, Michigan 48202, USA*
[17]*University of Bristol, Bristol BS8 1TL, UK*
[18]*Carleton University, Ottawa, Ontario, Canada K1S 5B6*
[19]*Carnegie Mellon University, Pittsburgh, Pennsylvania 15213, USA*
[20]*University of Chicago, Chicago, Illinois 60637, USA*
[21]*Cornell University, Ithaca, New York 14853, USA*
[22]*University of Florida, Gainesville, Florida 32611, USA*
[23]*George Mason University, Fairfax, Virginia 22030, USA*
[24]*University of Illinois, Urbana-Champaign, Illinois 61801, USA*
(Received 13 October 2010; published 22 December 2010)

We report the first determination of the relative strong-phase difference between $D^0 \to K^0_{S,L} K^+ K^-$ and $\bar{D}^0 \to K^0_{S,L} K^+ K^-$. In addition, we present updated measurements of the relative strong-phase difference between $D^0 \to K^0_{S,L} \pi^+ \pi^-$ and $\bar{D}^0 \to K^0_{S,L} \pi^+ \pi^-$. Both measurements exploit the quantum coherence between a pair of D^0 and $\bar{D}^0$ mesons produced from $\psi(3770)$ decays. The strong-phase differences measured are important for determining the Cabibbo-Kobayashi-Maskawa angle γ/ϕ_3 in $B^- \to K^- \tilde{D}^0$ decays, where $\tilde{D}^0$ is a D^0 or $\bar{D}^0$ meson decaying to $K^0_S h^+ h^-$ ($h = \pi, K$), in a manner independent of the model assumed to describe the $D^0 \to K^0_S h^+ h^-$ decay. Using our results, the uncertainty in γ/ϕ_3 due to the error on the strong-phase difference is expected to be between 1.7° and 3.9° for an analysis using $B^- \to K^- \tilde{D}^0$, $\tilde{D}^0 \to K^0_S \pi^+ \pi^-$ decays, and between 3.2° and 3.9° for an analysis based on $B^- \to K^- \tilde{D}^0$,

[*]Now at: Pacific Northwest National Laboratory, Richland, WA 99352, USA

$\tilde{D}^0 \to K^0_S K^+ K^-$ decays. A measurement is also presented of the CP-odd fraction, $\mathcal{F}_-$, of the decay $D^0 \to K^0_S K^+ K^-$ in the region of the $\phi \to K^+ K^-$ resonance. We find that in a region within 0.01 GeV$^2/c^4$ of the nominal ϕ mass squared $\mathcal{F}_- > 0.91$ at the 90% confidence level.

DOI: 10.1103/PhysRevD.82.112006 PACS numbers: 13.25.Ft, 12.15.Hh, 14.40.Lb

I. INTRODUCTION

A central goal of flavor physics is the determination of all elements of the Cabibbo-Kobayashi-Maskawa (CKM) matrix [1], both magnitudes and phases. Of the three angles of the $b - d$ CKM triangle, denoted α, β, and γ by some, ϕ_2, ϕ_1, and ϕ_3 by others, the least well determined is γ/ϕ_3, the phase of V_{cb} relative to V_{ub}. It is of great interest to determine γ/ϕ_3 using the decay $B^\pm \to K^\pm \tilde{D}^0$, since in this mode, the γ/ϕ_3 value is expected to be insensitive to new physics effects in B decay; here, $\tilde{D}^0$ is either a D^0 or $\bar{D}^0$ meson decaying to the same final state. This is in contrast with most measurements of CP violation, which are dominated by processes that have significant contributions from loop diagrams that can be influenced by new physics [2,3]. Therefore, precise measurements of γ/ϕ_3 from the decay $B^\pm \to K^\pm \tilde{D}^0$ compared to the predictions for γ/ϕ_3 from loop-dominated processes provide a stringent test of the origin of CP violation in the standard model. Sensitivity to the angle γ/ϕ_3 comes from the interference between two Cabibbo-suppressed diagrams: $b \to c\bar{u}s$, giving rise to $B^- \to K^- D^0$,[1] and the color and CKM suppressed process $b \to u\bar{c}s$, giving rise to $B^- \to K^- \bar{D}^0$ [4]. Promising $\tilde{D}^0$ decays for measuring γ/ϕ_3 using this method are $\tilde{D}^0 \to K^0_S \pi^+ \pi^-$ [5,6] and $\tilde{D}^0 \to K^0_S K^+ K^-$, here designated collectively as $\tilde{D}^0 \to K^0_S h^+ h^-$. To make use of these decays, however, it is necessary to understand the interference effects between $D^0 \to K^0_S h^+ h^-$ and $\bar{D}^0 \to K^0_S h^+ h^-$. These effects can be measured using CLEO-c data. A study of the decay $\tilde{D}^0 \to K^0_S \pi^+ \pi^-$ has already been published [7]. Here we present an update of that analysis, and first results from the decay $\tilde{D}^0 \to K^0_S K^+ K^-$.

Let us write the amplitude for the $B^- \to K^- \tilde{D}^0$, $\tilde{D}^0 \to K^0_S h^+ h^-$ decay as follows:

$$f_{B^-}(m^2_+, m^2_-) \propto f_D(m^2_+, m^2_-) + r_B e^{i(\delta_B - \gamma)} f_{\bar{D}}(m^2_+, m^2_-). \tag{1}$$

Here, m^2_+ and m^2_- are the invariant-mass squared of the $K^0_S h^+$ and $K^0_S h^-$ pairs from the $\tilde{D}^0 \to K^0_S h^+ h^-$ decay, which define the Dalitz plot, $f_D(m^2_+, m^2_-)(f_{\bar{D}}(m^2_+, m^2_-))$ is the amplitude for the $D^0(\bar{D}^0)$ decay to $K^0_S h^+ h^-$ at (m^2_+, m^2_-) in the Dalitz plot, r_B is the ratio of the suppressed to favored amplitudes, and δ_B is the strong-phase difference between the color-favored and color-suppressed amplitudes. Ignoring the second-order effects of charm mixing and CP violation in charm [5,8,9], we have $f_{\bar{D}}(m^2_+, m^2_-) = f_D(m^2_-, m^2_+)$, and Eq. (1) can then be written as

$$f_{B^-}(m^2_+, m^2_-) \propto f_D(m^2_+, m^2_-) + r_B e^{i(\delta_B - \gamma)} f_D(m^2_-, m^2_+). \tag{2}$$

The square of the amplitude clearly depends on the phase difference $\Delta\delta_D \equiv \delta_D(m^2_+, m^2_-) - \delta_D(m^2_-, m^2_+)$, where $\delta_D(m^2_+, m^2_-)$ is the phase of $f_D(m^2_+, m^2_-)$. Thus, for the determination of γ/ϕ_3, one must know $\Delta\delta_D$.

Analyses of $B^- \to K^- \tilde{D}^0$ decays to date extracted $\Delta\delta_D(m^2_+, m^2_-)$ for each final state by fitting flavor-tagged $D^0 \to K^0_S \pi^+ \pi^-$ [10–14] and $D^0 \to K^0_S K^+ K^-$ [12,14] Dalitz plots to D^0-decay models involving various two-body intermediate states. The systematic uncertainty associated with this modeling is hard to estimate; the assigned values vary between 3° and 9° for the more recent analyses. In order to exploit fully the high statistics expected at LHCb [15,16] and future e^+e^- B-factory experiments [17,18] it is highly desirable to avoid this modeling uncertainty, and to do it in a manner which keeps all other error sources small compared with the foreseen statistical precision.

In the analysis presented here, we employ a model-independent approach to obtain $\Delta\delta_D(m^2_+, m^2_-)$ as suggested in Refs. [5,19], by exploiting the quantum coherence of $D^0 - \bar{D}^0$ pairs at the $\psi(3770)$. Because of this quantum correlation, $K^0_S h^+ h^-$ and $K^0_L h^+ h^-$ decays recoiling against flavor tags, CP tags, and $D^0 \to K^0_S h^+ h^-$ tags, taken together, provide direct sensitivity to the quantities $\cos\Delta\delta_D$ and $\sin\Delta\delta_D$ for each final state. The analysis is performed in discrete bins of $D^0 \to K^0_S h^+ h^-$ Dalitz space. We have updated the $D^0 \to K^0_S \pi^+ \pi^-$ analysis reported in Ref. [7] by providing results in alternative sets of Dalitz-plot bins, and by reducing some of the systematic uncertainties.

In addition measurements of the time-dependent evolution of the $D^0 \to K^0_S h^+ h^-$ Dalitz plot provide some of the most precise constraints on charm-mixing parameters [20]. These measurements also rely on D^0-decay models that introduce significant systematic uncertainties. A model-independent determination of the charm-mixing parameters from $D^0 \to K^0_S h^+ h^-$ that uses the same strong-phase difference parameters as the γ/ϕ_3 analysis of B^- decay has been proposed [9]. The advantage of the model-independent approach is again the elimination of model-dependent assumptions about the strong-phase differences.

We also present the first model-independent measurement of the CP content of the decay $D^0 \to K^0_S K^+ K^-$ in the region of the $\phi \to K^+ K^-$ resonance. The decay

[1]Here and throughout this paper the charge-conjugate state is implied unless otherwise stated.

$D^0 \to K^0_S\phi$ is a CP-odd eigenstate and has been used as such in several analyses; see, for example, Refs. [21,22]. The $\phi \to K^+K^-$ resonance is usually defined by a mass window about the nominal ϕ mass. Despite its narrow natural width of 4.26 MeV/c^2 [23], the potential contributions from CP-even final states beneath the ϕ resonance, such as $D^0 \to K^0_S a_0(980)$ and nonresonant $D^0 \to K^0_S K^+K^-$ decays, must be accounted for. Using $D^0 \to K^0_{S,L}K^+K^-$ decays recoiling against CP eigenstates we determine the CP-odd fraction of decays, $\mathcal{F}_-$, in the region close to the ϕ resonance. A measurement of $\mathcal{F}_-$ allows a systematic uncertainty related to the CP-even contamination to $D^0 \to K^0_S\phi$ decays to be assigned without assuming an amplitude model for the decay $D^0 \to K^0_S K^+K^-$.

This paper is organized as follows. The formalism for the measurement of the strong-phase difference and $\mathcal{F}_-$ is outlined in Sec. II. The choice of Dalitz-plot bins is given in Sec. III. The event selection is described in Sec. IV. Sections V and VI present the extraction of the variables associated with the strong-phase differences and the assignment of systematic uncertainties, respectively. The impact of these results on the measurement of γ/ϕ_3 is discussed in Sec. VII, along with the measurement of $\mathcal{F}_-$. A summary is given in Sec. VIII. Throughout this article the $D^0 \to K^0_S\pi^+\pi^-$ and $D^0 \to K^0_S K^+K^-$ analyses are described in parallel, but more weight is given to the latter as it has not been presented previously.

II. FORMALISM

Giri *et al.* proposed [5] a model-independent procedure for obtaining $\Delta\delta_D(m^2_+, m^2_-)$ as follows. The Dalitz plot is divided into $2\mathcal{N}$ bins, symmetrically about the line $m^2_+ = m^2_-$. The bins are indexed with i, running from $-\mathcal{N}$ to $\mathcal{N}$ excluding zero. Thus, the coordinate exchange $m^2_+ \leftrightarrow m^2_-$ corresponds to the exchange of the bins $i \leftrightarrow -i$. The number of events (K_i) in the i^{th} bin of a flavor-tagged $K^0_S h^+h^-$ Dalitz plot from a D^0 decay is then expressed as

$$K_i = A_D \int_i |f_D(m^2_+, m^2_-)|^2 dm^2_+ dm^2_- = A_D F_i, \quad (3)$$

where the integral is performed over the i^{th} bin. Here A_D is a normalization factor and F_i is the fraction of $D^0 \to K^0_S h^+h^-$ events in the i^{th} bin. The interference between the D^0 and $\bar{D}^0$ amplitudes is parameterized by two quantities:

$$c_i \equiv \frac{1}{\sqrt{F_i F_{-i}}} \int_i |f_D(m^2_+, m^2_-)||f_D(m^2_-, m^2_+)| \times \cos[\Delta\delta_D(m^2_+, m^2_-)] dm^2_+ dm^2_-, \quad (4)$$

and

$$s_i \equiv \frac{1}{\sqrt{F_i F_{-i}}} \int_i |f_D(m^2_+, m^2_-)||f_D(m^2_-, m^2_+)| \times \sin[\Delta\delta_D(m^2_+, m^2_-)] dm^2_+ dm^2_-. \quad (5)$$

The parameters c_i and s_i are the amplitude-weighted averages of $\cos\Delta\delta_D$ and $\sin\Delta\delta_D$ over each Dalitz-plot bin.

Though the original idea of Giri *et al.* was to divide the Dalitz plot into square bins, Bondar and Poluektov noted [19] that alternative bin definitions will lead to significantly increased sensitivity. In particular, one can choose to minimize the variation in $\Delta\delta_D$ over each bin according to the predictions of one of the models developed on flavor-tagged data [10–14]. Note that this approach does *not* introduce a model dependence in the final result for γ/ϕ_3. This result will remain unbiased by the choice of an incorrect model, but will have less statistical sensitivity than expected. If we divide the Dalitz plot into $\mathcal{N}$ bins of equal size with respect to $\Delta\delta_D$ as predicted by one of these models, then in the half of the Dalitz plot $m^2_+ < m^2_-$, the i^{th} bin is defined by the condition

$$2\pi(i - 3/2)/\mathcal{N} < \Delta\delta_D(m^2_+, m^2_-) < 2\pi(i - 1/2)/\mathcal{N}, \quad (6)$$

and the $-i^{\text{th}}$ bin is defined symmetrically in the lower portion of the Dalitz plot. The choice of $D^0 \to K^0_S\pi^+\pi^-$ binning with $\mathcal{N} = 8$ as obtained from the model presented in Ref. [12] is shown in Fig. 1. A discussion on alternative choices of binning for $D^0 \to K^0_S\pi^+\pi^-$ and those for $D^0 \to K^0_S K^+K^-$ can be found in Sec. III.

We now describe how CLEO-c data can be used to determine c_i and s_i. The event yields in the i^{th} bin of both flavor-tagged and CP-tagged $\tilde{D}^0 \to K^0_S h^+h^-$ Dalitz plot are required. Because the $\psi(3770)$ has $C = -1$, the CP eigenvalue of one D meson can be determined by reconstructing the companion D meson in a CP eigenstate. With a CP-tagged $\tilde{D}^0 \to K^0_S h^+h^-$ decay, the amplitude is given by

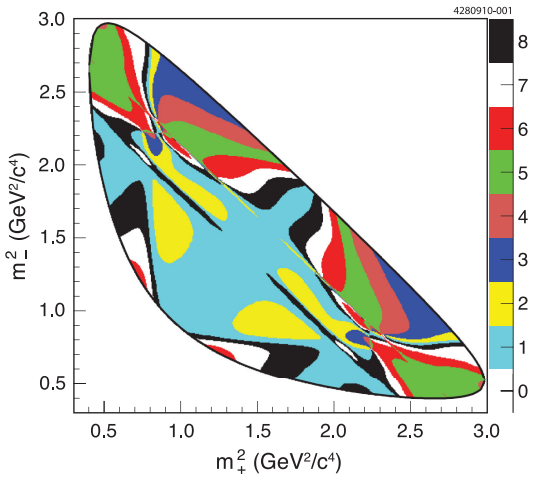

FIG. 1 (color online). Equal $\Delta\delta_D$ binning of the $D^0 \to K^0_S\pi^+\pi^-$ Dalitz plot with $\mathcal{N} = 8$ based on the model from Ref. [12]. The color scale represents the absolute value of the bin number, $|i|$.

$$f_{CP\pm}(m_+^2, m_-^2) = \frac{1}{\sqrt{2}}[f_D(m_+^2, m_-^2) \pm f_D(m_-^2, m_+^2)] \quad (7)$$

for CP-even $(+)$ and CP-odd $(-)$ states of a $\tilde{D}^0 \to K_S^0 h^+ h^-$ decay. Since the event rate is proportional to the square of this amplitude, the number of events in the i^{th} bin of a CP-even or CP-odd tagged Dalitz plot is then

$$M_i^{\pm} = h_{CP\pm}(K_i \pm 2c_i\sqrt{K_i K_{-i}} + K_{-i}), \quad (8)$$

where $h_{CP\pm} = S^{\pm}/2S_f$ is a normalization factor that depends on the number, S_f, of flavor-tagged signal decays, and the number, $S^{\pm}$, of D^0 mesons decaying to a CP eigenstate in the sample irrespective of the decay of the other D meson; this is referred to as a single-tagged (ST) sample. Alternatively the normalization factor can be defined in terms of branching fractions, $\mathcal{B}$, as $h_{CP^{\pm}} = \mathcal{B}_{CP^{\pm}}/2\mathcal{B}_f$, where $\mathcal{B}_{CP^{\pm}}$ $(\mathcal{B}_f)$ is the branching fraction of D^0 to CP eigenstates (flavor tags). Thus, access to c_i is enabled by measuring the number of events, $M_i^{\pm}$, in a CP-tagged $K_S^0 h^+ h^-$ Dalitz plot, and the number of events, K_i, in a flavor-tagged $K_S^0 h^+ h^-$ Dalitz plot.

Important additional information can be gained through analysis of $D^0 \to K_S^0 h^+ h^-$ vs. $\bar{D}^0 \to K_S^0 h^+ h^-$ data. The amplitude for $\psi(3770)$ decaying to a double $K_S^0 h^+ h^-$ final state is as follows:

$$f(m_+^2, m_-^2, m_+'^2, m_-'^2) = \frac{f_D(m_+^2, m_-^2) f_D(m_-'^2, m_+'^2) - f_D(m_+'^2, m_-'^2) f_D(m_-^2, m_+^2)}{\sqrt{2}}. \quad (9)$$

The primed and unprimed Dalitz-plot coordinates correspond to the Dalitz-plot variables of the two $\tilde{D}^0 \to K_S^0 h^+ h^-$ decays. Defining M_{ij} as the event rate in the i^{th} bin of the first and the j^{th} bin of the second $\tilde{D} \to K_S^0 h^+ h^-$ Dalitz plots, respectively, we have

$$M_{ij} = h_{\text{corr}}\Big(K_i K_{-j} + K_{-i} K_j - 2\sqrt{K_i K_{-j} K_{-i} K_j}(c_i c_j + s_i s_j)\Big). \quad (10)$$

Here, $h_{\text{corr}} = N_{D\bar{D}}/2S_f^2 = N_{D\bar{D}}/8\mathcal{B}_f^2$, where $N_{D\bar{D}}$ is the number of $D\bar{D}$ pairs, and as before S_f is the number of flavor-tagged signal decays. Thus analysis of both $D^0 \to K_S^0 h^+ h^-$ vs. $\bar{D}^0 \to K_S^0 h^+ h^-$ data and CP-tagged $D^0 \to K_S^0 h^+ h^-$ decays allows c_i and s_i to be determined. The ambiguity in the sign of s_i can be resolved using weak model assumptions.

The decay $D^0 \to K_L^0 h^+ h^-$, due to its close relations with $D^0 \to K_S^0 h^+ h^-$, can be used to improve further the c_i and s_i determination. We assume the convention that $A(D^0 \to K_S^0 h^+ h^-) = A(\bar{D}^0 \to K_S^0 h^- h^+)$. Then, since the K_S^0 and K_L^0 mesons are of opposite CP, it follows that $A(D^0 \to K_L^0 h^+ h^-) = -A(\bar{D}^0 \to K_L^0 h^- h^+)$. Hence for $K_L^0 h^+ h^-$ the Dalitz-plot rates of Eqs. (8) and (10) become

$$M_i'^{\pm} = h_{CP\pm}(K_i' \mp 2c_i'\sqrt{K_i' K_{-i}'} + K_{-i}'), \quad (11)$$

and

$$M_{ij}' = h_{\text{corr}}\Big(K_i K_{-j}' + K_{-i} K_j' + 2\sqrt{K_i K_{-j}' K_{-i} K_j'}(c_i c_j' + s_i s_j')\Big) \quad (12)$$

for CP vs. $D^0 \to K_L^0 h^+ h^-$ and $D^0 \to K_S^0 h^+ h^-$ vs. $\bar{D}^0 \to K_L^0 h^+ h^-$, respectively, where K_i' c_i', and s_i' are associated with the decay $D^0 \to K_L^0 h^+ h^-$. In the analysis all four parameters c_i, s_i, c_i', and s_i' are determined for each channel, but in order to improve the precision on c_i and s_i constraints are imposed on the differences $\Delta c_i \equiv c_i' - c_i$ and $\Delta s_i \equiv s_i' - s_i$. These constraints are discussed in Sec. V.

Because the branching fraction of $D^0 \to K^0 \pi^+ \pi^-$ is around 5 times larger than $D^0 \to K^0 K^+ K^-$ it is advantageous to first determine the coefficients c_i, s_i, c_i', and s_i' for the former decay, and then use these to help improve our knowledge of the coefficients for $D^0 \to K^0 K^+ K^-$. This is achieved through measuring the bin-by-bin rates for $K_S^0 K^+ K^-$ vs. $K_S^0 \pi^+ \pi^-$, $K_L^0 K^+ K^-$ vs. $K_S^0 \pi^+ \pi^-$, and $K_S^0 K^+ K^-$ vs. $K_L^0 \pi^+ \pi^-$ Dalitz plots, and using suitably modified forms of Eqs. (10) and (12).

The expression for the CP-odd fraction in the region of the $\phi \to K^+ K^-$ resonance in $D^0 \to K_S^0 K^+ K^-$ decays follows from Eq. (8). We note that $M_i^+ + M_i^- = M_{-i}^+ + M_{-i}^-$; in addition, this sum is proportional to $K_i + K_{-i}$, the total rate of $D^0 \to K_S^0 K^+ K^-$ decays in the combined i and $-i$ bins. Therefore, if bin i defines an interval of $K^+ K^-$ invariant-mass squared, $m_{K^+K^-}^2$, about the nominal ϕ mass squared, then the CP-odd fraction of $D^0 \to K_S^0 K^+ K^-$ decays, $\mathcal{F}_-$, in that region is

$$\mathcal{F}_- = \frac{M_i^- + M_{-i}^-}{M_i^- + M_{-i}^- + M_i^+ + M_{-i}^+}. \quad (13)$$

We determine $\mathcal{F}_-$ for four different invariant-mass squared intervals: 0.006, 0.010, 0.014, and 0.018 GeV^2/c^4.

III. DALITZ PLOT BIN DEFINITIONS

Measurements of $c_i^{(\prime)}$ and $s_i^{(\prime)}$ are presented for three and four alternative binnings for $D^0 \to K_S^0 K^+ K^-$ and $D^0 \to K_S^0 \pi^+ \pi^-$, respectively. The motivation for these choices and the resulting binning definitions are presented in this section.

A. Binnings of the $D^0 \to K_S^0 K^+ K^-$ Dalitz plot

We use an amplitude model determined by *BABAR* [14] for which a lookup table of the results in Dalitz space has

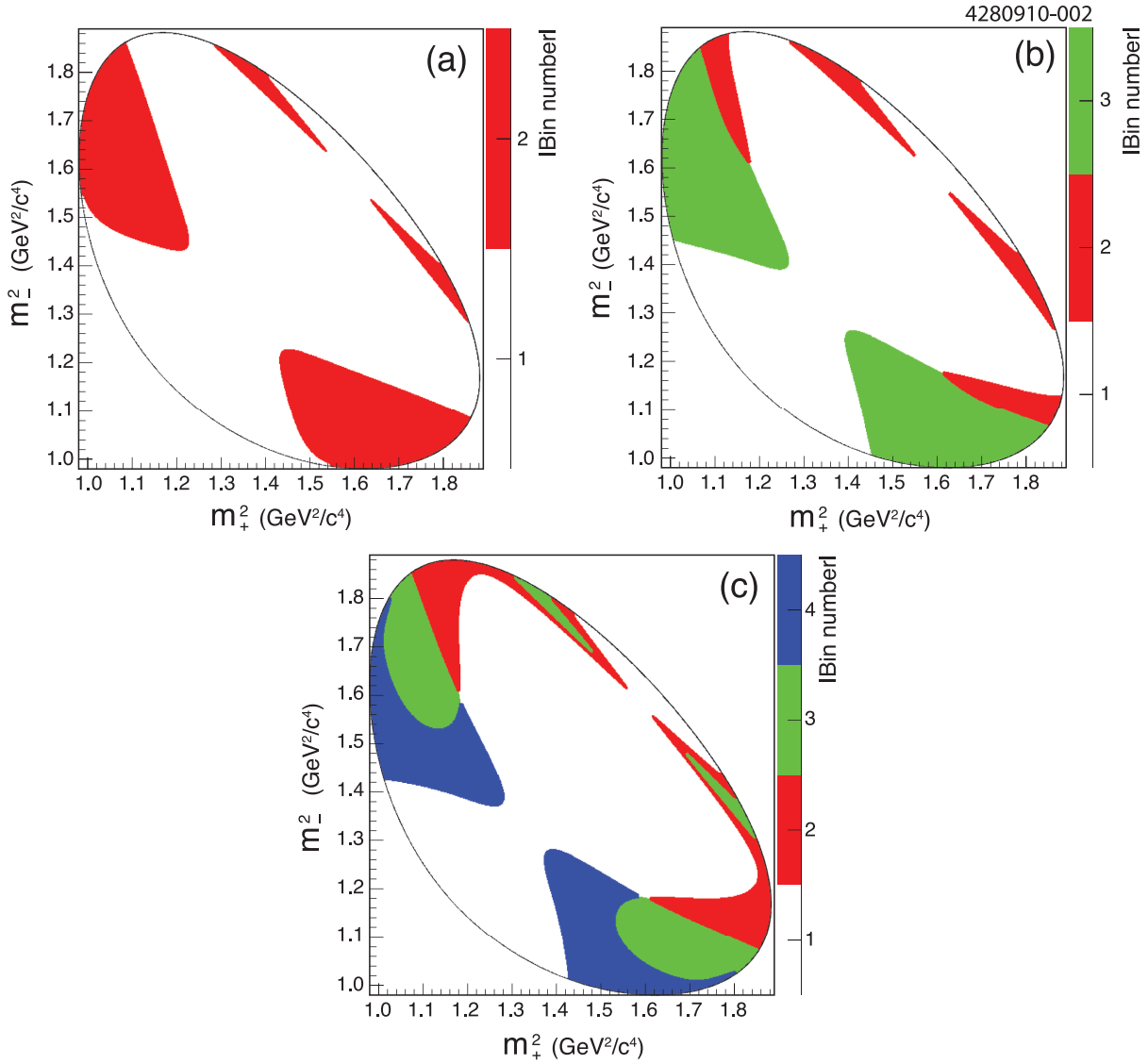

FIG. 2 (color online). Equal $\Delta\delta_D$ division of the $D^0 \to K^0_S K^+ K^-$ Dalitz plot into (a) $\mathcal{N} = 2$, (b) $\mathcal{N} = 3$, and (c) $\mathcal{N} = 4$ bins.

been provided by the authors [24]. The amplitude model uses the isobar formalism and consists of eight intermediate resonances, of which five are parameterized with Breit-Wigner line shapes and three, $a_0(980)^0 K^0_S$ and $a_0(980)^{\pm} K^{\mp}$, are parameterized by a coupled-channel Breit-Wigner function [25].

We consider binnings in which the Dalitz plane is divided into $\mathcal{N} = 2$, $\mathcal{N} = 3$, and $\mathcal{N} = 4$ equal $\Delta\delta_D$ bins, according to Eq. (6). A smaller number of bins provides superior statistical precision on the parameters associated with $\Delta\delta_D$ but a reduced sensitivity to γ. Using a larger number of bins is not feasible due to the limited statistics available in the CLEO-c data; the fit to the parameters (Sec. V) fails to converge if $\mathcal{N} > 4$. However, these alternatives will allow flexibility in matching an appropriate number of bins for the size of the available B-decay sample when the values c_i and s_i are used to extract γ.

The three cases considered are shown in Fig. 2. In each case, there is a narrow bin located at low values of $m^2_{K^+K^-}$, which is close to the diagonal boundary of the Dalitz plot. This bin encompasses the ϕ intermediate resonance and typically contains the largest number of events. For three and four bins there are "lobes" at high values of $m^2_{K^+K^-}$ that contain relatively few events.

B. Binnings of the $D^0 \to K^0_S \pi^+ \pi^-$ Dalitz plot

The four binnings used in the updated analysis of $D^0 \to K^0_S \pi^+ \pi^-$ are described in this section. The *BABAR* model [12] that is used to define the bin choices is described in Sec. III B 1. Then the binning in equal intervals of the strong-phase difference is presented in Sec. III B 2. In Sec. III B 3 the procedure to optimize the binning for maximal sensitivity to γ is described and the resulting

binning is presented. In Sec. III B 4 we describe a modified procedure of optimization which takes into account expected background levels at LHCb. In Sec. III B 5 the binning in equal intervals of the strong-phase difference as defined by the latest Belle model [13] is given. Finally, in Sec. III B 6 we summarize the differences between the various bin definitions and also assess what consequences a very recent *BABAR* $D^0 \to K^0_S\pi^+\pi^-$ model [14], not available originally for our analysis, would have for the bin definitions.

1. BABAR K-matrix model

The amplitude models used by Belle [10,13] and the first *BABAR* analysis [11] are parameterized in terms of a Breit-Wigner isobar model. However, the broad $\pi\pi$ and $K\pi$ S-wave components are not well described by such Breit-Wigner line shapes. In particular an additional intermediate state, σ', is required to fit the $\pi\pi$ S wave even though it is known not to be a physical resonance. Furthermore, parameterizing these broad overlapping states in terms of Breit-Wigner functions is unphysical in that unitarity can be violated. Therefore, a more recent *BABAR* model [12] uses the K-matrix [26] ansatz to parameterize the $\pi\pi$ S-wave contributions, which does not violate unitarity. In addition, the empirical LASS line shape [27] of the $K^*_0(1430)$ is used to improve the fit to the $K\pi$ S-wave component. We refer to this approach as the *BABAR 2008 model*. The reduced χ^2 for the *BABAR* 2008 model fit to the $D^{*+} \to D^0\pi^+$ data is significantly improved over the first *BABAR* model [11] and is much better than that for the Belle model. Therefore, this model was considered the best available and is used to define the nominal binnings implemented in this analysis. The results of the model have been made available by the *BABAR* Collaboration in the form of a lookup table of the amplitude and strong-phase difference, δ_D, in a fine grid of $0.0054\ \mathrm{GeV}^2/c^4 \times 0.0054\ \mathrm{GeV}^2/c^4$ sub-bins of the Dalitz plot variables $m^2_\pm$ [24]. The $m^2_\pm$ resolution, estimated from simulation, is of the same order as the sub-bin dimensions; the resolution is $0.006\ \mathrm{GeV}^2/c^4$ $(0.015\ \mathrm{GeV}^2/c^4)$ for $D^0 \to K^0_S\pi^+\pi^-$ $(D^0 \to K^0_L\pi^+\pi^-)$. [The lookup table for $D^0 \to K^0_SK^+K^-$ has a grid of $0.0018\ \mathrm{GeV}^2/c^4 \times 0.0018\ \mathrm{GeV}^2/c^4$ sub-bins. The resolution is $0.005\ \mathrm{GeV}^2/c^4$ $(0.010\ \mathrm{GeV}^2/c^4)$ for $D^0 \to K^0_SK^+K^-$ $(D^0 \to K^0_LK^+K^-)$.]

Since performing the analysis of the CLEO-c data using the bin choices described here, which are based on the *BABAR* 2008 model, a new *BABAR* measurement [14] has been published which presents an updated version of the $D^0 \to K^0_S\pi^+\pi^-$ decay model that we term the *BABAR 2010 model*. This model is derived from a larger data sample that has been reprocessed and the analysis has been improved with respect to experimental systematic uncertainties. In Sec. III B 6 we assess the consequences on the bin choices of the differences between the two models and conclude that they are minor.

2. Equal $\Delta\delta_D$ binning of the BABAR 2008 model

The first binning of the Dalitz space for the *BABAR* 2008 model we consider follows the proposal in Ref. [19], which was used in the previous CLEO-c analysis [7] and in the analysis of $D^0 \to K^0_SK^+K^-$. The binning is such that there are $\mathcal{N} = 8$ bins of $\Delta\delta_D$ in each half the Dalitz plot as defined in Eq. (6). This equal $\Delta\delta_D$ binning for the *BABAR* 2008 model is shown in Fig. 1.

3. Optimal binning of the BABAR 2008 model

Following Ref. [19] the ratio of sensitivity to γ/ϕ_3 of a binned compared to an unbinned method is given by

$$Q^2 = \frac{\sum_i \left[\left(\frac{1}{\sqrt{\Gamma_i}}\frac{d\Gamma_i}{dx}\right)^2 + \left(\frac{1}{\sqrt{\Gamma_i}}\frac{d\Gamma_i}{dy}\right)^2\right]}{\int\left[\left(\frac{1}{\sqrt{|f_{B^-}|^2}}\frac{d|f_{B^-}|^2}{dx}\right)^2 + \left(\frac{1}{\sqrt{|f_{B^-}|^2}}\frac{d|f_{B^-}|^2}{dy}\right)^2\right]dm^2_+\,dm^2_-}, \tag{14}$$

where

$$\Gamma_i = \int_i |f_{B^-}|^2 dm^2_+\,dm^2_-. \tag{15}$$

Here, f_{B^-} is expressed as

$$f_{B^-} = f_D(m^2_+, m^2_-) + (x + iy) f_D(m^2_-, m^2_+), \tag{16}$$

where $x = r_B\cos(\delta_B - \gamma)$ and $y = r_B\sin(\delta_B - \gamma)$. The parameter, Q, is the ratio of the number of standard deviations difference in the yields of $B^- \to K^-\tilde{D}^0$ events as x and y change in a finite number of bins with respect to an infinite number of bins. The sensitivity to x and y is largely independent of their values. Therefore, again following Ref. [19], Eq. (14) can be simplified assuming $x = y = 0$ to become

$$Q^2|_{x=y=0} = \frac{\sum_i N_i(c_i^2 + s_i^2)}{\sum_i N_i}, \tag{17}$$

where N_i is the number of $B^- \to K^-\tilde{D}^0(K^0_S\pi^+\pi^-)$ events in the i^{th} bin when r_B is zero. Recalling that c_i and s_i are the amplitude-weighted averages of $\cos\Delta\delta_D$ and $\sin\Delta\delta_D$ over each bin, respectively, it is clear that regions of similar $\Delta\delta_D$ will yield reasonable, though not necessarily optimal, values of Q. The Q value of the equal $\Delta\delta_D$ binning presented in Sec. III B 2 is 0.786 indicating that this binning choice is over 20% less sensitive statistically than an unbinned approach. (The values of Q are also computed for the different $D^0 \to K^0_SK^+K^-$ binnings reported in Sec. III A; the values are 0.771, 0.803, and 0.822 for $\mathcal{N} = 2$, $\mathcal{N} = 3$, and $\mathcal{N} = 4$ equal $\Delta\delta_D$ binnings, respectively.)

In Ref. [19] it was shown that the binning can be optimized to increase the value of Q. The optimization algorithm was provided by the authors of Ref. [19] and was adapted to use the lookup table of the *BABAR* 2008 model. The optimization is iterative and starts from the equal $\Delta\delta_D$

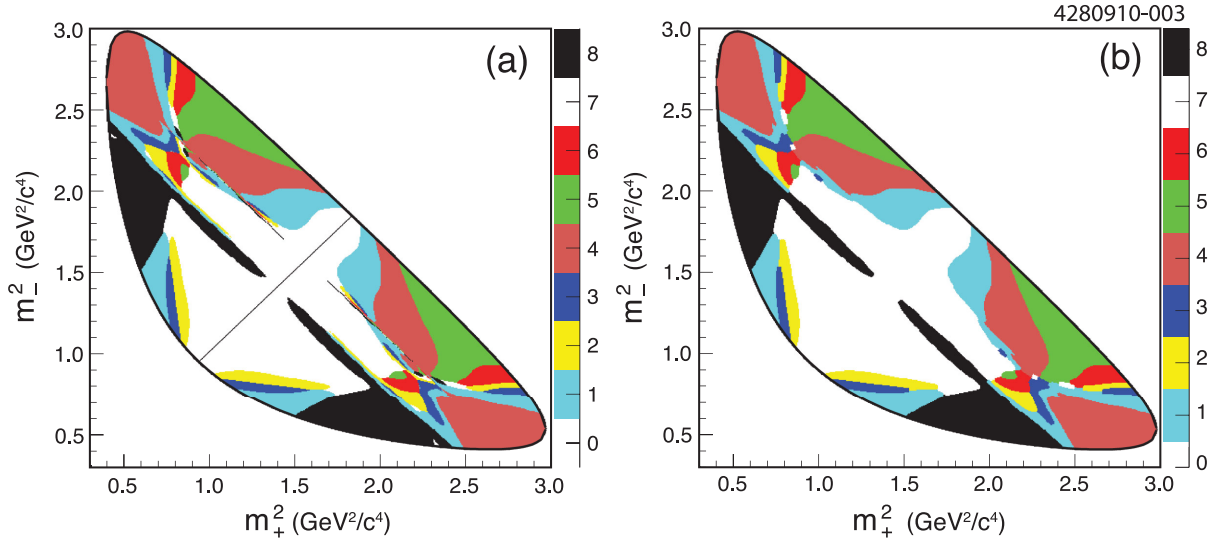

FIG. 3 (color online). (a) Optimal binning of the $D^0 \to K^0_S\pi^+\pi^-$ Dalitz plot that was found to exploit best the B statistics according to the *BABAR* 2008 model. (b) The same binning after the smoothing procedure described in the text has been applied. The color scale represents the value $|i|$.

binning presented in Sec. III B 2. Each iteration starts with the random selection of a sub-bin from the lookup table. In 90% of iterations the sub-bin is first tested to see if it lies on the boundary of a bin. If the sub-bin is not at a boundary the next iteration begins. Otherwise the sub-bin is moved from its current assignment to that of the neighboring bin and the value of Q is computed with the new assignment. If the value of Q is increased by this migration, the new assignment for this bin is kept and the next iteration begins. If the value of Q does not increase the assignment reverts to that originally given and the next iteration begins. In 10% of iterations, the selected sub-bin is given an assignment at random, irrespective of whether it is on a bin boundary. Again the reassignment of the sub-bin is kept if there is an improvement in Q; this allows part of one bin to "grow" inside another bin if there is an improvement in the sensitivity. The procedure terminates when no further significant increase in the value of Q can be found.

The binning that results from this optimization procedure is shown in Fig. 3(a) and is significantly different from that of the equal $\Delta\delta_D$ binning (Fig. 1). The optimized Q value is 0.892, which is a 13% relative increase in sensitivity. However, there are many structures that are only a few sub-bins in size. Such regions are smaller than the experimental resolution and may result in systematic effects related to asymmetric migration of events from one bin to another. Furthermore, the position and shape of this fine structure depends critically on the components in the model, which may be realized differently in nature. Therefore, a smoothing procedure is implemented to remove these structures. The smoothing procedure starts by defining an 11×11 square of sub-bins centered about the sub-bin that is being tested. The number of sub-bins with the same bin assignment as the central sub-bin within the square is found. If the fraction of sub-bins of the same assignment is less than 30% the sub-bin assignment is changed to the modal bin assignment within the square. This procedure is performed for each sub-bin with the bin assignments from the original optimization to prevent bias. Figure 3(b) shows the binning after this smoothing procedure; the value of Q only decreases by 0.005. The smoothed optimal binning is used to calculate $c_i^{(\prime)}$ and $s_i^{(\prime)}$.

The same optimization procedure is applied to the three $D^0 \to K^0_S K^+ K^-$ binnings in terms of equal intervals of $\Delta\delta_D$. However, the improvements in Q are found to be negligible compared to the equal binnings. Therefore, the $c_i^{(\prime)}$ and $s_i^{(\prime)}$ parameters for $D^0 \to K^0_S K^+ K^-$ decay are not reported here for optimized binnings.

4. Modified-optimal binning of the BABAR 2008 model for the presence of background

The Q values for the binnings provided are computed assuming that there is no background present. There is a clear advantage to using the optimal binning in such a case, and simulation studies of a measurement of γ using the observed values of c_i, s_i, and the number of flavor-tagged $D^0 \to K^0_S\pi^+\pi^-$ events in each bin, K_i, have confirmed the improved sensitivity in comparison to the equal $\Delta\delta_D$ binning. However, when background is added to the simulation studies the sensitivity to γ using the optimal binning can be worse than that for the equal $\Delta\delta_D$ binning (see Sec. VII). The addition of background events naturally reduces the sensitivity to γ. The measurement of γ is most sensitive when there are significant differences between yields in the bins for positive and negative B decays. In simulations there are two observed effects that can dilute the sensitivity. For the optimal binning there are

bins where the asymmetry is large while the expected yields are low. If there is a large background yield in such a bin then the size of the asymmetry can be diluted to the point where the sensitivity gained by the optimal binning choice is significantly reduced by the presence of background. Also, very large bins contain a large fraction of the combinatoric background, which follows a reasonably uniform distribution over the Dalitz plot, which dilutes the asymmetry in that bin. With an assumed background model, it is possible to find a binning choice that maximizes the sensitivity to γ in the presence of background.

The background model assumed is determined from simulation studies of LHCb described in Ref. [16]. In this work three distinct types of background are considered. The first type of background is pure combinatoric, where the D^0 is reconstructed from a random combination of pions; the background-to-signal ratio, B/S, is expected to be less than 1.1 at the 90% confidence level. The second type of background is where a D meson is reconstructed correctly, and is then subsequently combined with a random kaon candidate to form a B candidate. The reconstruction of the D^0 and $\bar{D}^0$ is approximately equally likely and hence the distribution of this type of background in the i^{th} bin will be proportional to $(K_i + K_{-i})$. For this type of background, B/S is expected to be 0.35 ± 0.03. The third type of background, which has the smallest contribution to the total background, involves real B decays, predominantly $B^- \to \pi^- \tilde{D}^0$ where the pion is misidentified as a kaon. In total the real B background has B/S less than 0.24 at the 90% confidence level. Sensitivity studies have shown that this type of background causes only a minor degradation in the sensitivity to γ. Therefore, this background type is ignored. In summary, the data sample is assumed to be composed of 41% signal events, 45% combinatoric background and 14% fully reconstructed D background.

In the presence of background the calculation of Q changes and will be written as Q' to distinguish it from the no background case. The value of Q' is still related to the number of standard deviations by which the number of events in each bin is changed by varying parameters x and y, to the number of standard deviations if the Dalitz plot is divided into infinitely small regions as defined in Eq. (14), however the definition of $|f_{B^-}|^2$ is now

$$|f_{B^-}|^2 = f_s|f_D(m_+^2, m_-^2) + (x + iy)f_D(m_-^2, m_+^2)|^2 + f_1\mathcal{B}_1(m_+^2, m_-^2) + f_2\mathcal{B}_2(m_+^2, m_-^2), \quad (18)$$

where $\mathcal{B}_1(m_+^2, m_-^2)$ and $\mathcal{B}_2(m_+^2, m_-^2)$ are the probability density functions for the combinatoric and fully reconstructed D backgrounds, respectively, and f_s, f_1, and f_2 are the fractions of signal, combinatoric background, and fully reconstructed D backgrounds, respectively. The assumed values of f_s, f_1 and f_2 are 0.41, 0.45, and 0.14.

As before the precision of x and y weakly depends on their values, therefore, the simplification that $x = y = 0$ is once more made. In this case the expression analogous to Eq. (17) is given by

$$Q'^2|_{x=y=0} = \frac{\sum_i \frac{f_s^2 F_i F_{-i}}{f_s F_i + f_1 B_{1i} + f_2 B_{2i}}(c_i^2 + s_i^2)}{\int \frac{f_s^2|f_D(m_+^2,m_-^2)|^2|f_D(m_-^2,m_+^2)|^2}{f_s|f_D(m_+^2,m_-^2)|^2 + f_1\mathcal{B}_1 + f_2\mathcal{B}_2} dm_+^2\, dm_-^2}, \quad (19)$$

where B_{1i} (B_{2i}) is the integrated probability density functions for the combinatoric (fully reconstructed D) background over the i^{th} bin.

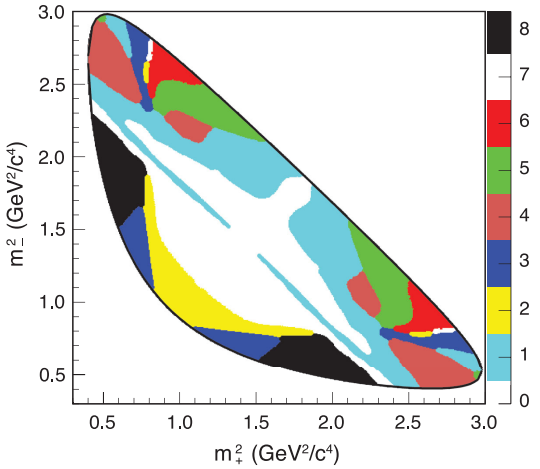

FIG. 4 (color online). Modified-optimal binning of the $D^0 \to K_S^0\pi^+\pi^-$ Dalitz plot based on the *BABAR* 2008 model. The color scale represents the absolute value of the bin number, $|i|$.

The optimization algorithm to find the modified-optimal binning with the highest Q' is the same as described in Sec. III B 3. The modified-optimal binning Q' value is 0.910. In comparison, the equal $\Delta\delta_D$ binning has $Q' = 0.882$ and the optimal binning has $Q' = 0.867$. The fine structure of the binning is smoothed out using the same technique as described for the optimal binning; the Q' value drops by 0.006. The binning after the smoothing procedure is given in Fig. 4. In addition, we performed studies that show this binning choice retains the highest values of Q' even when the assumptions of the background model are modified. The alternative background models tested contain combinatoric background with a B/S between 0.8 and 1.3, and fully reconstructed D^0 background with a B/S between 0.26 and 0.44.

5. Belle model binning

The shape of the bins are dependent on the details of the amplitude model for the decay. There is another model available from the Belle experiment with which to define the bins [13]. This model does not use the same descriptions of the $\pi\pi$ and $K\pi$ S wave as the *BABAR* 2008 and 2010 models [12,14]. A lookup table of this model has been provided by the Belle Collaboration [28]. Therefore, for a completeness, and to cross check our baseline results derived from the *BABAR* 2008 model, an equal $\Delta\delta_D$

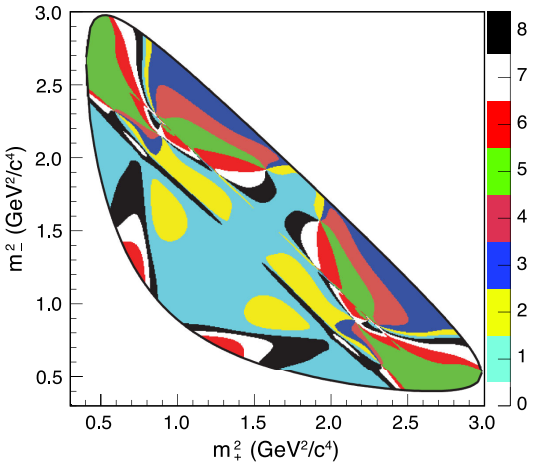

FIG. 5 (color online). Equal $\Delta\delta_D$ binning of the $D^0 \to K^0_S\pi^+\pi^-$ Dalitz plot with $\mathcal{N} = 8$ based on the Belle model [13]. The color scale represents the absolute value of the bin number, $|i|$.

interval binning is derived from the latest Belle model. The binning over the Dalitz space is given in Fig. 5.

6. Bin choice comparisons and the BABAR 2010 model

The 2010 *BABAR* model only became available [24] after the completion of the $D^0 \to K^0_S\pi^+\pi^-$ analysis. Therefore, to determine the possible impact on γ/ϕ_3 precision related to differences between the 2008 and 2010 models we compute the values of the respective figure of merit, Q or Q', for each *BABAR* model. This is done with the binnings fixed to those described above, which are derived from the *BABAR* 2008 model or the Belle model. The resulting figures of merit are given in Table I for the 2008 and 2010 *BABAR* models; the values of $Q^{(\prime)}$ are also given when computed with the Belle model. The values of $Q^{(\prime)}$ computed using the *BABAR* 2010 model are slightly smaller than those for the 2008 model, but the difference is never greater than 0.007. In comparison, when calculating $Q^{(\prime)}$ with the Belle model, for binnings derived from the *BABAR* 2008 model, the decrease is between 0.018 and 0.030. Therefore, we conclude that using the *BABAR* 2008 model, rather than the *BABAR* 2010 model, to derive the binnings in this analysis will not result in a significant degradation in sensitivity to γ/ϕ_3.

IV. EVENT SELECTION

This section summarizes the event selection for the two analyses. Section IV A describes the selection of $D^0 \to K^0_{S,L}K^+K^-$ events. Section IV B briefly summarizes the changes to the selection of $D^0 \to K^0_{S,L}\pi^+\pi^-$ events with respect to the previous analysis [7].

A. Selection of $D^0 \to K^0_{S,L}K^+K^-$

We perform the analysis on e^+e^- collision data produced by the Cornell Electron Storage Ring at a center-of-mass energy, $E_{\rm cm}$, of 3.77 GeV. The data were collected by the CLEO-c detector and correspond to an integrated luminosity of 818 pb^{-1}. The CLEO-c detector is a solenoidal detector which includes a gaseous tracking system for the measurement of charged particle momenta and ionization energy loss, a ring-imaging Cherenkov detector to aid in particle identification, and a CsI crystal calorimeter to measure the energy of electromagnetic showers. The CLEO-c detector is described in detail elsewhere [29].

Samples of Monte Carlo (MC) simulated data are used to develop selection criteria, determine selection efficiencies, and to estimate certain types of background. EVTGEN [30] is used to generate the decays and GEANT [31] is used to simulate the CLEO-c detector response. Efficiency estimations are made on samples of signal events generated according to the $D^0 \to K^0_SK^+K^-$ resonance model reported in Ref. [12]. Separate signal samples are generated for each exclusive final state considered in the analysis and comprise 40 000 events per final state. Quantum correlations in the $D^0\bar{D}^0$ system are also simulated for each tag mode; this is particularly important for the CP-tagged D^0 decays. In addition a sample of generic $D\bar{D}$ decays corresponding to an integrated luminosity approximately 25 times greater than the data is used to estimate backgrounds. Quantum correlations are accounted for in the generic simulation.

We adopt standard CLEO-c selection criteria for π^+, π^0, and K^0_S mesons, which are described in Ref. [32]. The standard CLEO-c K^+ selection [32] is used for all final states apart from $D^0 \to K^0_{S,L}K^+K^-$. For this final state, which has much smaller yields than $K^0_{S,L}\pi^+\pi^-$, the significance of the signal is found to increase if the impact parameter criteria are loosened by a factor of 4 and

TABLE I. Comparison of the figure of merit values (Q, Q') calculated using the different models.

Binning	Figure of merit	*BABAR* 2008 [12]	*BABAR* 2010 [14]	Belle [13]
Equal $\Delta\delta_D$	Q	0.786	0.780	0.762
Optimal	Q	0.887	0.880	0.857
Modified optimal	Q'	0.904	0.903	0.886
Belle	Q	0.754	0.755	0.773

TABLE II. Single-tag and $D^0 \to K^0_{S,L} h^+ h^-$ double-tag yields. The single tag yields and uncertainties are computed following the method reported in Ref. [7] and are not corrected for efficiency. The DT yields are the observed number of events in the signal region prior to background subtraction and before efficiency correction.

Mode	ST yield	DT yields			
		$K^0_S\pi^+\pi^-$	$K^0_L\pi^+\pi^-$	$K^0_S K^+ K^-$	$K^0_L K^+ K^-$
Flavor tags					
$K^-\pi^+$	144 563 ± 403	1444	2857	168	302
$K^-\pi^+\pi^0$	258 938 ± 581	2759	5133	330	585
$K^-\pi^+\pi^+\pi^-$	220 831 ± 541	2240	4100	248	287
$K^- e^+ \nu$		1191		100	
CP-even tags					
K^+K^-	13 349 ± 128	124	357	12	32
$\pi^+\pi^-$	6177 ± 114	61	184	4	13
$K^0_S\pi^0\pi^0$	6838 ± 134	56		7	14
$K^0_L\pi^0$		237		17	
$K^0_L\eta(\gamma\gamma)$				4	
$K^0_L\eta(\pi^+\pi^-\pi^0)$				1	
$K^0_L\omega$				4	
$K^0_L\eta'$				1	
CP-odd tags					
$K^0_S\pi^0$	19 753 ± 153	189	288	18	43
$K^0_S\eta(\gamma\gamma)$	2886 ± 71	39	43	4	6
$K^0_S\eta(\pi^+\pi^-\pi^0)$				2	1
$K^0_S\omega$	8830 ± 110	83		14	10
$K^0_S\eta'$				3	4
$K^0_L\pi^0\pi^0$				5	
$K^0_S\pi^+\pi^-$		473	1201	56	126
$K^0_L\pi^+\pi^-$				140	
$K^0_S K^+ K^-$				4	9

the requirement on the fraction of associated tracking chamber hits compared to the expectation is removed. We require candidate $K^0_S \to \pi^+\pi^-$ decays to have a mass within 7.5 MeV/c^2 of the nominal mass and the K^0_S decay vertex is required to be separated from the interaction region by at least half a standard deviation. We reconstruct $\eta \to \gamma\gamma$ candidates in a similar fashion to $\pi^0 \to \gamma\gamma$ candidates, with the requirement that the invariant mass is within 42 MeV/c^2 of the nominal mass; the same requirement is applied to $\eta \to \pi^+\pi^-\pi^0$ candidates. Candidates for $\omega \to \pi^+\pi^-\pi^0$ decays are required to be within 20 MeV/c^2 of the nominal ω mass. We require $\eta' \to \eta\pi^+\pi^-$ candidates to have an invariant mass in the range 950 to 964 MeV/c^2. All nominal masses are taken from Ref. [23].

We consider $K^0_{S,L}K^+K^-$ candidates reconstructed against the different final states listed in Table II. These are referred to as double-tagged (DT) events. More *CP*-tagged final states are used in the analysis of $K^0_{S,L}K^+K^-$ than the $K^0_{S,L}\pi^+\pi^-$ analysis [7] to increase the statistics available to determine c_i for this decay. (These modes are not included in the analysis of $K^0_S\pi^+\pi^-$ because in this measurement the principal statistical limitation is the number of $K^0_S\pi^+\pi^-$ vs. $K^0_{L,S}\pi^+\pi^-$ events used to determine s_i.) We do not reconstruct final states containing two missing particles, such as $K^0_L K^+ K^-$ vs. $K^0_L\pi^0$.

Final states that do not contain a K^0_L meson or neutrino are fully reconstructed via two kinematic variables: the beam-constrained candidate mass, $m_{bc} \equiv \sqrt{E^2_{\rm cm}/(4c^4) - \mathbf{p}^2_D/c^2}$, where $\mathbf{p}_D$ is the D candidate momentum, and $\Delta E \equiv E_D - E_{\rm cm}/2$, where E_D is the sum of the D daughter candidate energies. Signal decays will peak at the nominal D^0 mass and zero in m_{bc} and ΔE, respectively. Mode-dependent requirements are placed on $K^0_S K^+ K^-$ and tag candidates such that ΔE is less than 3 standard deviations from zero. The DT yield is determined from counting events in signal and sideband regions of the

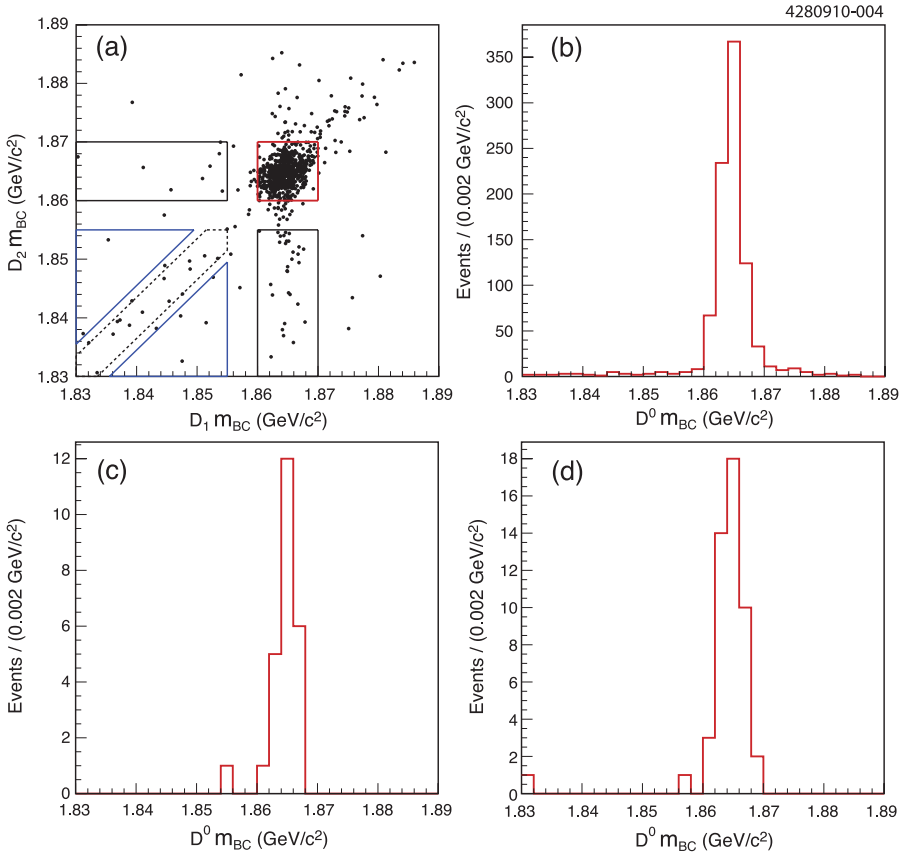

FIG. 6 (color online). (a) Distribution of m_{bc} for $D^0 \to K^0_S K^+ K^-$ candidates (D_1) against the m_{bc} for flavor-tag candidates (D_2): $\bar{D}^0 \to K^+\pi^-$, $K^+\pi^-\pi^0$ and $K^+\pi^-\pi^-\pi^+$. The square signal region (red online) and four sideband regions are shown. Distributions of m_{bc} for $D^0 \to K^0_S K^+ K^-$ candidates tagged by (b) flavor, (c) CP-even, and (d) CP-odd decays.

$(m_{bc}(D^0), m_{bc}(\bar{D}^0))$ plane in a manner similar to that presented in Refs. [21,33]. The signal region is defined as $1.86\ \mathrm{GeV}/c^2 < m_{bc}(D^0) < 1.87\ \mathrm{GeV}/c^2$ and $1.86\ \mathrm{GeV}/c^2 < m_{bc}(\bar{D}^0) < 1.87\ \mathrm{GeV}/c^2$. An example of the two-dimensional distribution of $(m_{bc}(D^0), m_{bc}(\bar{D}^0))$ is shown in Fig. 6(a) for $K^0_S K^+ K^-$ candidates reconstructed against $K^+\pi^-$, $K^+\pi^-\pi^0$, and $K^+\pi^-\pi^-\pi^+$ decays. The four different sidebands contain contributions from distinct types of combinatorial background. The yields in these sidebands are scaled and subtracted from the yield in the signal region. The m_{bc} distributions for $\tilde{D}^0 \to K^0_S K^+ K^-$ candidates tagged by flavor, CP-even, and CP-odd final states are shown in Figs. 6(b)–6(d), respectively. These figures show clearly that the combinatorial backgrounds are small. The background-to-signal ratio for combinatoric background is less than 7.3% for all modes.

To identify final states containing a single K^0_L meson, we compute the missing-mass squared recoiling against the fully reconstructed D candidate and the particles from the other D decay containing the K^0_L meson. We select events consistent with the mass of the K^0_L meson squared. This technique was introduced in Ref. [34]. We reject events with additional charged tracks, π^0, and η candidates that are unassigned to the final state of interest. In addition, requirements are placed on any calorimeter energy deposits not associated with the charged or neutral particles that make up the final state of interest. The angle, α, between each unassigned shower and the missing-momentum direction is computed. Criteria are chosen to maximize signal sensitivity based on simulated samples of signal and background events. We retain events where $\cos\alpha \geq 0.98$, which indicates that the deposit is likely to be due to the interaction of the K^0_L meson with the calorimeter. When $\cos\alpha < 0.98$ mode-by-mode requirements are placed on the unassociated shower energy. The unassociated shower energy is required to be below a certain value which varies from 200 MeV for $D^0 \to K^0_L\pi^0\pi^0$ candidates to 370 MeV for $D^0 \to K^0_L\omega$ and $D^0 \to K^0_L\eta'$ candidates. Finally, criteria are placed on the momenta of π^0 and η candidates in tags containing a K^0_L meson to reduce background further. The combinatoric background yield in the signal region is estimated from the population in the lower and upper missing-mass squared sidebands. Information from the generic background simulation is used to determine the relative composition of the sidebands and the signal region to estimate better the combinatorial background. Figure 7 is the distribution of missing-mass squared for CP-tagged $D^0 \to K^0_S K^+ K^-$ candidates for data and simulated

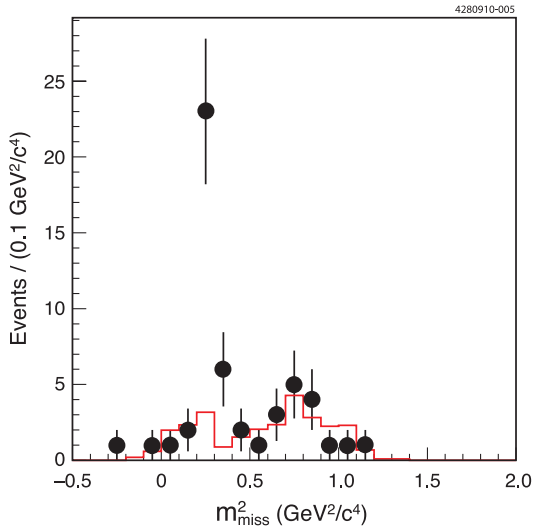

FIG. 7 (color online). Missing-mass squared distribution for CP-tagged $D^0 \to K^0_S K^+ K^-$ candidates where the CP eigenstate contains a K^0_L meson. The points are data and the solid histogram is the background estimated from simulation.

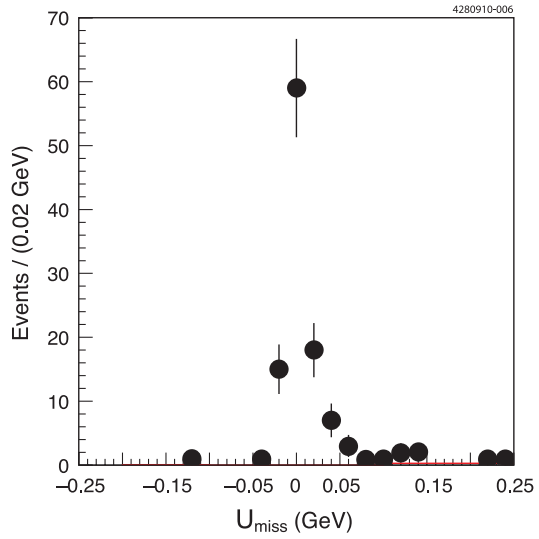

FIG. 8 (color online). $U_{\rm miss}$ distribution for $K^+ e^- \nu$-tagged $K^0_S K^+ K^-$ candidates. The points are data and the solid histogram is the background estimated from simulation. The background histogram (red online) is barely visible indicating that the background is negligible.

background, where the CP eigenstate used to tag the event contains a K^0_L meson.

We reconstruct the final state $\bar{D}^0 \to K^+ e^- \nu$ by fully reconstructing a $\tilde{D}^0 \to K^0_S K^+ K^-$ candidate and requiring that the rest of the event contains both a kaon and an electron candidate of opposite charge. The quantity $U_{\rm miss} \equiv E_{\rm miss} - c|\mathbf{p}_{\rm miss}|$ is used as a discriminating variable, where $E_{\rm miss}$ and $\mathbf{p}_{\rm miss}$ are the missing energy and momentum in the event, determined using the momenta of the fully reconstructed particles. The neutrino is the only particle not detected, so for a correctly reconstructed event $U_{\rm miss}$ will equal zero. Figure 8 is the distribution of $U_{\rm miss}$ in the data and simulated background. The DT event yields for all final states are given in Table II.

There are backgrounds to the signal that peak in m_{BC} and missing-mass squared at the same values as the signal, which can not be evaluated by examining the sidebands. These peaking backgrounds are estimated from the generic $D\bar{D}$ MC data samples. The largest peaking background to $D^0 \to K^0_S K^+ K^-$ decays is from $D^0 \to K^+ K^- \pi^+ \pi^-$ decays where the $\pi^+ \pi^-$ pair form a K^0_S candidate. The peaking background from this source is estimated to be approximately 3.2% of the signal. For $D^0 \to K^0_L K^+ K^-$ decays there are two significant peaking background contributions. The first source is $D^0 \to K^0_S K^+ K^-$ decays where the K^0_S is not reconstructed, usually in the case where it decays to $\pi^0 \pi^0$. The second significant source is from $D^0 \to K^+ K^- \pi^0 \pi^0$ decays where both the π^0 daughters are not reconstructed and the missing mass corresponds to that of the K^0_L meson. This background is not strictly peaking in that the $\pi^0 \pi^0$ invariant mass does not always correspond to that of the K^0_L meson. However, the missing-mass squared distribution for $D^0 \to K^+ K^- \pi^0 \pi^0$ background events determined from simulated data is not distributed linearly in the signal region and low missing-mass squared sideband, which would lead to a biased estimate of the background level if the sideband is used to determine the background level in the signal region. Therefore, the absolute level of this background is determined from the simulation and subtracted from both the signal and low missing-mass squared sideband. The $D^0 \to K^0_S K^+ K^-$ and $D^0 \to K^+ K^- \pi^0 \pi^0$ peaking backgrounds are estimated to be 6.7% and 4.4% of the $D^0 \to K^0_L K^+ K^-$ signal, respectively. Tag modes that contain a K^0_L, $\bar{D}^0 \to K^0_L X$, also have a significant peaking background from $\bar{D}^0 \to K^0_S X$ decays where the K^0_S is not reconstructed. The peaking background to $\bar{D}^0 \to K^0_L X$ events is between 4.0% and 6.9%. The estimated peaking backgrounds are subtracted from the measured yields. The differing CP eigenvalues of the $\bar{D}^0 \to K^0_S X$ and $\bar{D}^0 \to K^0_L X$ tags means that the distributions over Dalitz space of the signal and background can be significantly different. The effect of differing distributions of background is treated as a systematic uncertainty; the procedure to evaluate the uncertainty is described in Sec. VI B. The background to $K^+ e^- \nu$ events is estimated as 1.8% in the signal region, defined as $U_{\rm miss} < 50$ MeV.

We apply a kinematic fit to determine more reliably the position of a candidate in the Dalitz space. For final states containing a $D^0 \to K^0_S K^+ K^-$ decay, the fit constrains the invariant mass of both the signal and tag D^0 meson candidates to be the nominal D^0 mass and the K^0_S daughters to the nominal K^0_S mass. For $D^0 \to K^0_L K^+ K^-$ decays there are several stages to the fit. The first stage constrains both

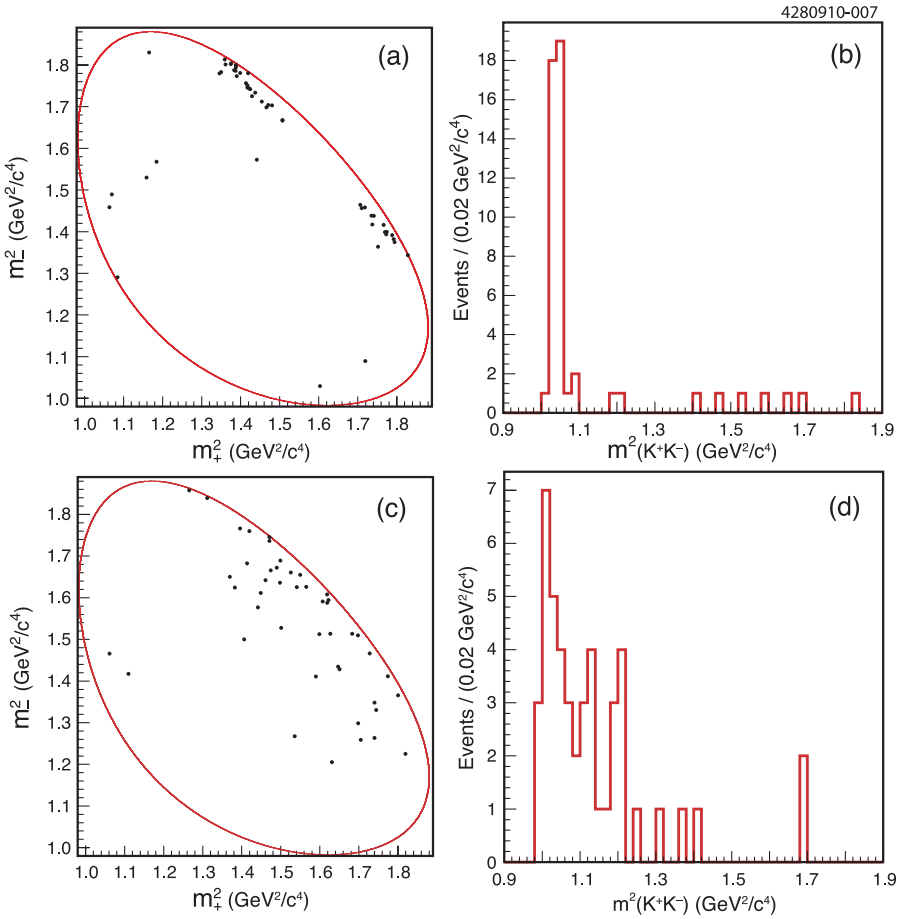

FIG. 9 (color online). (a) Dalitz plot and (b) $m^2_{K^+K^-}$ distributions of $D^0 \to K^0_S K^+ K^-$ candidates tagged by a CP-even eigenstate. (c) Dalitz plot and (d) $m^2_{K^+K^-}$ distributions of $D^0 \to K^0_S K^+ K^-$ candidates tagged by a CP-odd eigenstate.

the D^0 daughter kaons in the $D^0 \to K^0_L K^+ K^-$ decay to originate from a common vertex and the tag decay candidate to the D^0 mass. The second stage uses the resulting four-momenta to estimate the mass of the missing K^0_L meson. The energy of the K^0_L candidate is rescaled such that the invariant mass is the nominal K^0_L meson mass. In the final stage the K^0_L candidate and the daughter kaon pair are constrained to the nominal D^0 meson mass. The introduction of the kinematic fit improves the resolution on m^2_+ and m^2_- by up to a factor of 3 for fully reconstructed $K^0_S K^+ K^-$ DT candidates. Although the fit only gives small improvements in core resolution for K^0_L final states there is a significant reduction in the number of events that lie in the non-Gaussian tails of the resolution distribution.

The kinematic fit fails to converge in 1% to 3% of events, depending on the decay mode. In these cases the measured values of m^2_+ and m^2_- are rescaled such that they give the nominal D^0 mass. Even after the fit a small fraction of events are reconstructed outside the kinematic boundaries of the Dalitz space. The amplitude model used to assign events to a bin is undefined outside the Dalitz space. Therefore, the invariant masses of the candidate are changed to correspond to the point in the Dalitz space that is closest to the measured value in terms of the sum of $(\Delta m^2_+)^2$ and $(\Delta m^2_-)^2$, where $\Delta m^2_\pm$ is the residual between the measured value and a point within the Dalitz plot.

The distributions of events across the Dalitz plane and as a function of $m^2_{K^+K^-}$ for $K^0_S K^+ K^-$ reconstructed against CP-even tags are shown in Fig. 9. In addition, Fig. 9 shows the distributions across the Dalitz plane and as a function of $m^2_{K^+K^-}$ for $K^0_S K^+ K^-$ candidates reconstructed against CP-odd tags. The equivalent distributions for $K^0_L K^+ K^-$ candidates reconstructed against a CP eigenstate are shown in Fig. 10. The $m^2_{K^+K^-}$ distribution of $K^0_S K^+ K^-$ ($K^0_L K^+ K^-$) candidates tagged with CP-even (CP-odd) eigenstates exhibits a peak due to the ϕ resonance; as expected from CP conservation, this peak is not present for $K^0_S K^+ K^-$ ($K^0_L K^+ K^-$) candidates tagged with CP-odd (CP-even) eigenstates. Figure 11 shows the distribution of events across the Dalitz plane and as a function of $m^2_{K^+K^-}$ for $K^0_S K^+ K^-$ candidates reconstructed against $K^0_S \pi^+ \pi^-$ decays. Furthermore, Fig. 11 shows the distribution of the same events across the $K^0_S \pi^+ \pi^-$ Dalitz plane and as a function of the $\pi^+ \pi^-$ invariant-mass squared, $m^2_{\pi^+\pi^-}$. The increased statistics available from using events in which both D

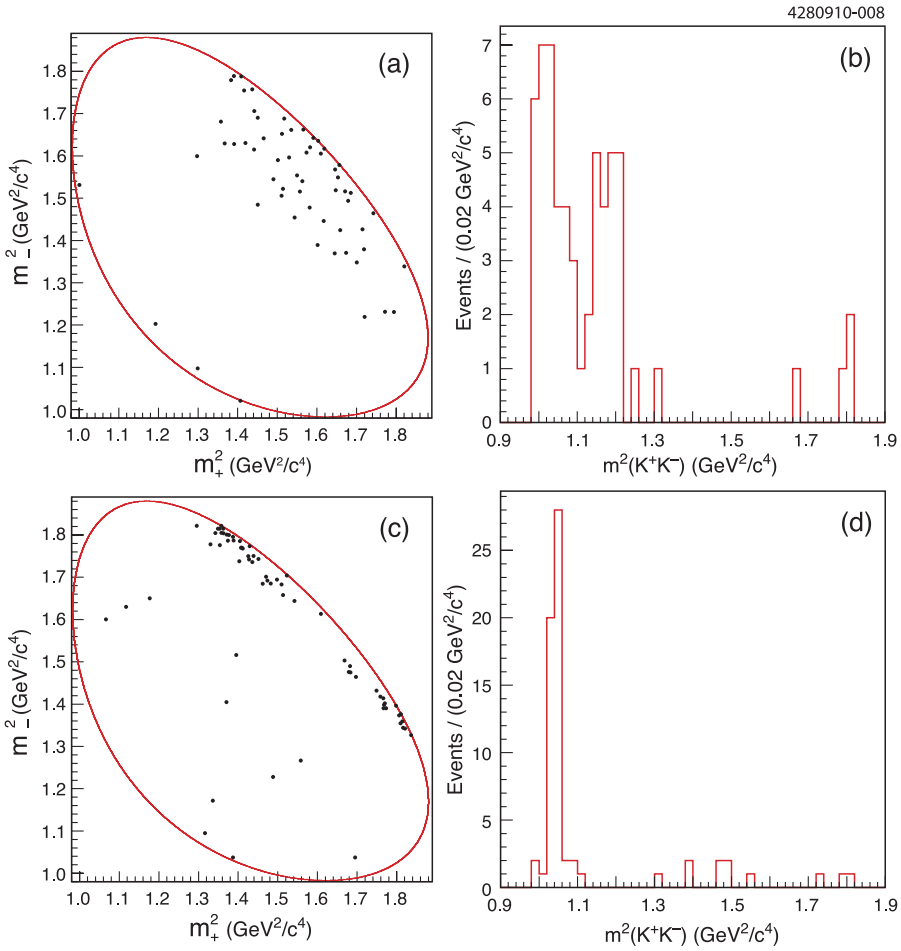

FIG. 10 (color online). (a) Dalitz plot and (b) $m^2_{K^+K^-}$ distributions of $D^0 \to K^0_L K^+ K^-$ candidates tagged by a CP-even eigenstate. (c) Dalitz plot and (d) $m^2_{K^+K^-}$ distributions of $D^0 \to K^0_L K^+ K^-$ candidates tagged by a CP-odd eigenstate.

mesons decay to $K^0_{S,L} h^+ h^-$ is clear. The distributions of flavor-tagged $D^0 \to K^0_S K^+ K^-$ and $D^0 \to K^0_L K^+ K^-$ candidates across the Dalitz plane and as a function of the $m_{K^+K^-}$ are shown in Fig. 12. The flavor-tagged samples are used to determine $K_i^{(\prime)}$ for each Dalitz-plot bin.

The efficiency in each bin is evaluated from the signal MC for each individual tag mode. Table III gives the total efficiency for each tag mode; these vary between $(0.51 \pm 0.04)\%$ for $K^0_S K^+ K^-$ vs. $K^0_L \pi^0 \pi^0$ to $(29.4 \pm 0.3)\%$ for $K^0_L K^+ K^-$ vs. $\pi^+ \pi^-$. The uncertainty on the efficiency is that due to MC statistics.

The finite detector resolution causes events to migrate between Dalitz-plane bins after reconstruction. Occasionally there is a significant asymmetric migration from one bin to another. The effect is more pronounced in $K^0_{S,L} K^+ K^-$ decays than in $K^0_{S,L} \pi^+ \pi^-$ decays because of the presence of a relatively narrow and densely populated bin that encloses the $\phi \to K^+ K^-$ resonance. We correct for this migration using MC data to determine the size and nature of the effect. For each binning we define a $2\mathcal{N} \times 2\mathcal{N}$ matrix $\mathbf{U}$ for each DT mode as follows:

$$U_{i,j} \equiv \frac{m_{j,i}}{\sum_{k=-\mathcal{N},k\neq 0}^{\mathcal{N}} m_{j,k}}, \tag{20}$$

where $m_{j,i}$ is the number of signal MC events that are generated in bin j and reconstructed in bin i. The vector of migration-corrected yields in each bin, $\mathbf{D}^{\rm corr}$, is determined from the vector of reconstructed yields in each bin, $\mathbf{D}^{\rm rec}$, using the relation:

$$\mathbf{D}^{\rm corr} = \mathbf{U}^{-1}\mathbf{D}^{\rm rec}. \tag{21}$$

As an example the migration matrix for $K^0_L K^+ K^-$ vs. $K^0_S \pi^0$ events when the $D^0 \to K^0_S K^+ K^-$ Dalitz space is divided into $\mathcal{N} = 3$ bins is given in Table IV. Typically the migration out of the bin containing the ϕ resonance is 5% for $D^0 \to K^0_S K^+ K^-$ modes and between 10% to 25% for $D^0 \to K^0_L K^+ K^-$ modes. The errors on the elements of $\mathbf{U}$ due to the limited MC statistics are treated as a systematic uncertainty.

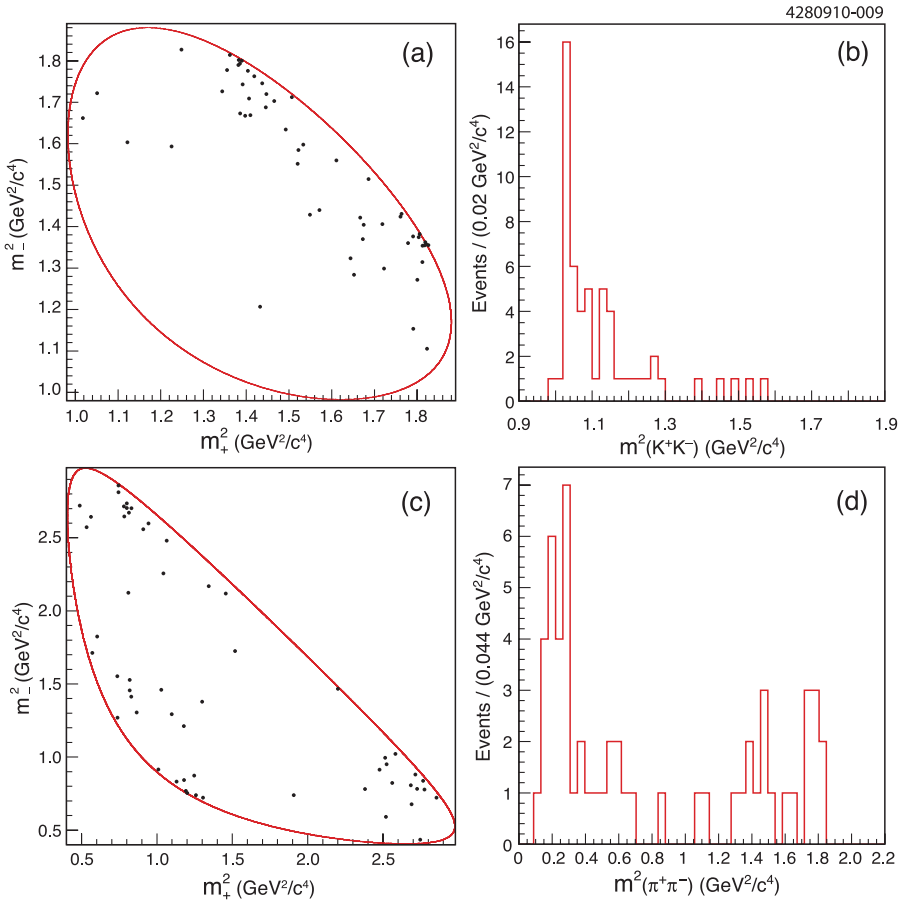

FIG. 11 (color online). (a) Dalitz plot and (b) $m^2_{K^+K^-}$ distributions of $D^0 \to K^0_S K^+ K^-$ candidates tagged by $\bar{D}^0 \to K^0_S \pi^+ \pi^-$ decays. (c) Dalitz plot and (d) $m^2_{\pi^+\pi^-}$ distributions of the $D^0 \to K^0_S \pi^+ \pi^-$ candidates in the same events.

B. Updates to the $K^0_{S,L}\pi^+\pi^-$ selection

Single tags are used in the analysis of $D^0 \to K^0_S \pi^+ \pi^-$ to determine the normalization factors in Eqs. (8) and (12) with limited systematic uncertainties. (In the $D^0 \to K^0_S K^+ K^-$ analysis these systematic uncertainties are not as important given the available statistics and therefore the normalizations are determined from the number of $D\bar{D}$ pairs and the measured branching fractions.) The ST selection is identical to that described in Ref. [7]. However, an error in the previous analysis led to a small fraction (3.6%) of the data being excluded from the ST analysis of CP eigenstates. The updated yields are given in Table II.

The selection requirements of DTs are identical to that in the previous analysis [7]. However, there are several changes to the yields reported. The same data excluded from the original ST analysis were missing from the evaluation of yields of final states containing a K^0_L candidate.[2] Also, the kinematic fit procedure described in Sec. IV A has also been applied to the $K^0\pi^+\pi^-$ events. However, events that lie outside the Dalitz plot after the fit procedure are rejected rather than migrated into the physical region, which changes some of the yields compared to those reported in Ref. [7]; in the previous analysis all events were retained. The updated DT yields are shown in Table II.

V. EXTRACTION OF c_i AND s_i

The efficiency-corrected, background-subtracted, and migration-corrected bin yields for each DT mode need to be normalized to determine the measured values of $M_i^{(\prime)\pm}$ and $M_{ij}^{(\prime)}$ so that they can be used to evaluate $c_i^{(\prime)}$ and $s_i^{(\prime)}$ via Eqs. (8) and (10)–(12). In addition, the values of flavor-tagged yields in each bin must also be normalized appropriately to obtain $K_i^{(\prime)}$. For the $K^0_S K^+ K^-$ analysis the single-tag yields in the normalization factors h_{CP} and $h_{\rm corr}$ in Eqs. (8) and (10)–(12) are determined from the number of $D^0\bar{D}^0$ pairs in the sample, $N_{D^0\bar{D}^0}$, multiplied by the branching fractions of the modes taken from Ref. [23]. The value of $N_{D^0\bar{D}^0}$ is calculated from the integrated luminosity and the value of the cross section for $e^+e^- \to \psi(3770) \to D^0\bar{D}^0$ reported in Ref. [32]. For the $K^0_{S,L}\pi^+\pi^-$ analysis the measured single-tag yields are

[2]In addition, the yields of $K^0_S\pi^+\pi^-$ vs. $K^-e^+\nu$ and $K^0_S\pi^+\pi^-$ vs. $K^0_S\pi^+\pi^-$ were incorrectly documented in Table II of Ref. [7].

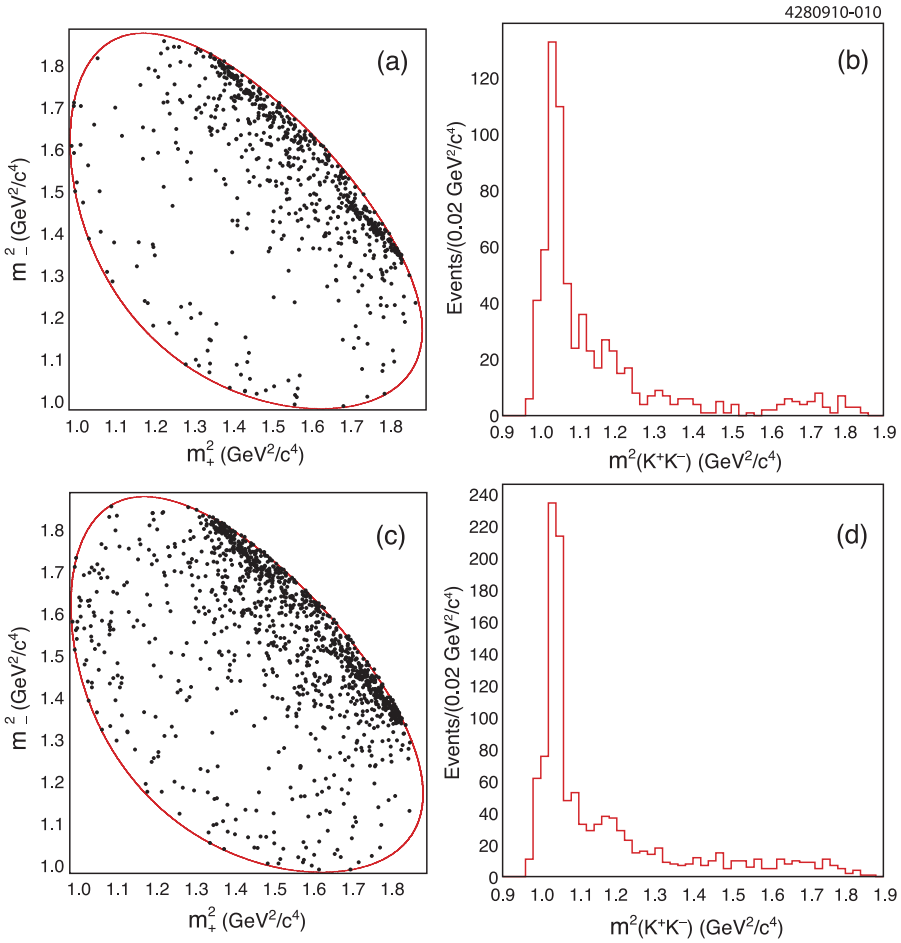

FIG. 12 (color online). (a) Dalitz plot and (b) $m^2_{K^+K^-}$ distributions of flavor-tagged $D^0 \to K^0_S K^+ K^-$ candidates. (c) Dalitz plot and (d) $m^2_{K^+K^-}$ distributions of flavor-tagged $D^0 \to K^0_L K^+ K^-$ candidates.

used for all modes apart from those tagged by $D^0 \to K^0_L \pi^0$ and $D^0 \to K^- e^+ \nu$, which cannot be reconstructed exclusively; in these cases the normalization is performed as in the $D^0 \to K^0_{S,L} K^+ K^-$ analysis.

Yields of $K^0_{S,L} h^+ h^-$ events selected against Cabibbo-favored hadronic flavor tags are contaminated with doubly Cabibbo suppressed (DCS) decays. We refer to these hadronic flavor modes as *pseudoflavor tags*. This introduces a bias in the extracted values of $K_i^{(\prime)}$ [7]. To account for this effect, the flavor-tagged yields in each bin are scaled by a correction factor, which is estimated using the $D^0 \to K^0_{S,L} K^+ K^-$ and $D^0 \to K^0_{S,L} \pi^+ \pi^-$ decay models reported in Refs. [11,14], respectively. The correction factor for pseudoflavor tag, $F \in (K^-\pi^+, K^-\pi^+\pi^0, K^-\pi^+\pi^+\pi-)$, is

$$\frac{\int_i |f(m^2_+, m^2_-)|^2 dm^2_+ dm^2_-}{\int_i (|f(m^2_+, m^2_-)|^2 + (r^F_D)^2 |f(m^2_-, m^2_+)|^2 + 2 r^F_D R_F \Re[e^{-i\delta^F_D} f(m^2_+, m^2_-) f^*(m^2_-, m^2_+)]) dm^2_+ dm^2_-}, \tag{22}$$

where r^F_D is the ratio of the DCS to Cabibbo-favored decay amplitudes and δ^F_D is the associated average strong-phase difference. R_F is the coherence factor for decays to three or more particles [35] and equals unity for two-body decays. The values of these parameters and the references from which they are taken are given in Table V.

Equation (3) defines $F_{(-)i}$, the normalized values of the flavor-tagged yields in each bin, such that $F_{(-)i} = K_{(-)i}/A_D$, where $A_D = \sum_{i=1}^{\mathcal{N}} (K_i + K_{-i})$. The fully corrected values of $F_{(-)i}$ measured for the $\mathcal{N} = 2$, $\mathcal{N} = 3$, and $\mathcal{N} = 4$ equal $\Delta\delta_D$ binnings are given in Table VI. The results are the average of the pseudoflavor tag modes with the $D^0 \to K^- e^+ \nu$ tagged data. Also given are the predicted values for $F_{(-)i}$ from the *BABAR* 2010 amplitude model of $D^0 \to K^0_S K^+ K^-$ decays. The error on the predicted value of $F_{(-)i}$ is determined from the

TABLE III. Selection efficiency for the different DT $K^0_{S,L}K^+K^-$ modes. The uncertainty is that due to MC simulation statistics.

Tag	Efficiency (%)	
	$K^0_SK^+K^-$	$K^0_LK^+K^-$
Flavor tags		
$K^-\pi^+$	14.6 ± 0.2	25.2 ± 0.3
$K^-\pi^+\pi^0$	8.5 ± 0.2	14.3 ± 0.2
$K^-\pi^+\pi^+\pi^-$	10.8 ± 0.2	15.9 ± 0.2
$K^-e^+\nu$	11.9 ± 0.2	
CP-even tags		
K^+K^-	12.2 ± 0.2	23.7 ± 0.3
$\pi^+\pi^-$	15.1 ± 0.2	29.4 ± 0.3
$K^0_S\pi^0\pi^0$	2.8 ± 0.1	5.9 ± 0.1
$K^0_L\pi^0$	8.0 ± 0.1	
$K^0_L\eta(\gamma\gamma)$	7.9 ± 0.1	
$K^0_L\eta(\pi^+\pi^-\pi^0)$	1.6 ± 0.1	
$K^0_L\omega$	3.1 ± 0.1	
$K^0_L\eta'$	1.7 ± 0.1	
CP-odd tags		
$K^0_S\pi^0$	7.1 ± 0.1	10.6 ± 0.2
$K^0_S\eta(\gamma\gamma)$	6.5 ± 0.1	9.7 ± 0.2
$K^0_S\eta(\pi^+\pi^-\pi^0)$	4.4 ± 0.1	6.8 ± 0.1
$K^0_S\omega$	3.4 ± 0.1	5.0 ± 0.1
$K^0_S\eta'$	1.4 ± 0.1	2.0 ± 0.1
$K^0_L\pi^0\pi^0$	0.51 ± 0.04	
$K^0_S\pi^+\pi^-$	7.9 ± 0.1	13.0 ± 0.2
$K^0_L\pi^+\pi^-$	14.0 ± 0.2	
$K^0_SK^+K^-$	4.9 ± 0.1	7.0 ± 0.1

TABLE IV. Migration matrix **U** elements (%) for $K^0_LK^+K^-$ vs. $K^0_S\pi^0$ events when the $D^0 \to K^0_LK^+K^-$ Dalitz space is divided into $\mathcal{N} = 3$ bins.

i	$U_{i,1}$	$U_{i,2}$	$U_{i,3}$	$U_{i,-1}$	$U_{i,-2}$	$U_{i,-3}$
1	86.2	11.8	0.5	0.4	0.0	0.0
2	11.3	88.1	0.5	0.0	0.0	0.0
3	1.5	0.1	98.9	0.0	0.0	0.0
−1	1.0	0.1	0.0	85.2	10.6	0.0
−2	0.0	0.0	0.0	13.9	89.3	1.0
−3	0.0	0.0	0.0	0.4	0.1	99.0

TABLE V. Values of the parameters used to make the corrections to the pseudoflavor tag yields and the references from which they are taken.

F	r^F_D (%)	δ^F_D (°)	R_F
$K\pi$	5.80 ± 0.08 [36]	202 ± 10 [36]	1
$K\pi\pi^0$	4.8 ± 0.2 [37]	227 ± 17 [21]	0.84 ± 0.07 [21]
$K\pi\pi\pi$	5.7 ± 0.2 [37]	114 ± 26 [21]	0.33 ± 0.26 [21]

TABLE VI. Values of $F_{(-)i}$ (%) measured from the flavor-tagged $D^0 \to K^0_SK^+K^-$ data for the $\mathcal{N} = 2$, $\mathcal{N} = 3$, and $\mathcal{N} = 4$ equal $\Delta\delta_D$ binnings. Predicted values from the *BABAR* 2010 model of $D^0 \to K^0_SK^+K^-$ are also given.

i	F_i (%)		F_{-i} (%)	
	Measured	Predicted	Measured	Predicted
	$\mathcal{N} = 2$ equal $\Delta\delta_D$ binning			
1	23.9 ± 1.6	22.5 ± 4.2	35.5 ± 1.9	28.6 ± 1.1
2	17.3 ± 1.5	21.1 ± 1.2	23.3 ± 1.7	27.8 ± 4.1
	$\mathcal{N} = 3$ equal $\Delta\delta_D$ binning			
1	22.0 ± 1.5	19.8 ± 3.8	33.0 ± 1.7	25.6 ± 1.0
2	18.1 ± 1.4	22.7 ± 1.4	22.8 ± 1.6	26.1 ± 5.3
3	1.2 ± 0.4	1.4 ± 0.7	3.0 ± 0.6	3.8 ± 1.6
	$\mathcal{N} = 4$ equal $\Delta\delta_D$ binning			
1	20.0 ± 1.5	18.3 ± 3.3	30.5 ± 1.7	23.0 ± 1.1
2	7.2 ± 1.1	8.5 ± 1.0	7.6 ± 1.3	8.6 ± 1.3
3	13.3 ± 1.4	16.3 ± 1.3	17.7 ± 1.4	21.3 ± 4.0
4	0.8 ± 0.4	0.5 ± 0.4	2.8 ± 0.6	3.5 ± 1.3

TABLE VII. Values of $F_{(-)i}$ (%) measured from the flavor-tagged $D^0 \to K^0_S\pi^+\pi^-$ data for the optimal binning. Predicted values from the *BABAR* 2008 model of $D^0 \to K^0_S\pi^+\pi^-$ are also given.

i	F_i (%)		F_{-i} (%)	
	Measured	Predicted	Measured	Predicted
1	17.0 ± 0.5	17.2	8.3 ± 0.4	8.3
2	8.4 ± 0.4	8.4	2.4 ± 0.2	1.9
3	7.2 ± 0.3	6.9	2.3 ± 0.2	2.0
4	2.4 ± 0.2	2.5	1.6 ± 0.2	1.7
5	7.6 ± 0.4	8.6	4.8 ± 0.3	5.3
6	5.9 ± 0.3	5.9	1.3 ± 0.2	1.5
7	12.8 ± 0.5	12.4	1.6 ± 0.2	1.4
8	13.0 ± 0.5	13.0	3.1 ± 0.2	2.8

uncertainties on the amplitude-model parameters. The agreement between the measured and predicted values is reasonable in all bins except F_{-1}, which is different by more than 3 standard deviations for all binnings. This discrepancy may be a statistical fluctuation or indicate a deficiency in the model in this region. In order to ascertain whether this effect can lead to a significant bias in our analysis, we perform the fit to determine $c_i^{(\prime)}$ and $s_i^{(\prime)}$ with the predicted rather than measured values of $K_{(-)i}$; the difference in fit results is negligible. Therefore, we conclude it is reasonable to use our measured values of $K_{(-)i}$ to determine the parameters. Tables VII, VIII, IX, and X show the measured values of $F_{(-)i}$ for the $D^0 \to K^0_S\pi^+\pi^-$ data divided according to the optimal, *BABAR* 2008 model with equal $\Delta\delta_D$, modified-optimal, and Belle equal $\Delta\delta_D$ binnings, respectively. Again these results are the average of pseudoflavor and semileptonic tagged data. Predicted

TABLE VIII. Values of $F_{(-)i}$ (%) measured from the flavor-tagged $D^0 \to K^0_S\pi^+\pi^-$ data for the equal $\Delta\delta_D$ binning derived from the *BABAR* 2008 model. Predicted values from the *BABAR* 2008 model of $D^0 \to K^0_S\pi^+\pi^-$ are also given.

i	F_i (%)		F_{-i} (%)	
	Measured	Predicted	Measured	Predicted
1	9.0 ± 0.4	9.1	2.6 ± 0.2	2.2
2	14.4 ± 0.5	14.2	0.5 ± 0.1	0.5
3	14.7 ± 0.5	14.1	0.3 ± 0.1	0.4
4	9.9 ± 0.4	10.0	5.9 ± 0.3	6.6
5	5.7 ± 0.3	5.4	3.3 ± 0.2	3.2
6	7.5 ± 0.4	7.4	0.5 ± 0.1	0.4
7	10.9 ± 0.4	11.5	5.5 ± 0.3	5.4
8	2.2 ± 0.2	2.2	6.9 ± 0.3	6.3

TABLE IX. Values of $F_{(-)i}$ (%) measured from the flavor-tagged $D^0 \to K^0_S\pi^+\pi^-$ data for the modified-optimal binning. Predicted values from the *BABAR* 2008 model of $D^0 \to K^0_S\pi^+\pi^-$ are also given.

i	F_i (%)		F_{-i} (%)	
	Measured	Predicted	Measured	Predicted
1	5.4 ± 0.3	5.1	1.5 ± 0.2	1.6
2	16.0 ± 0.5	16.2	2.1 ± 0.3	2.0
3	22.0 ± 0.6	21.6	2.3 ± 0.3	2.1
4	7.8 ± 0.4	8.8	4.9 ± 0.5	5.3
5	3.8 ± 0.3	3.9	3.1 ± 0.4	2.8
6	8.3 ± 0.4	8.1	1.1 ± 0.2	1.2
7	8.7 ± 0.4	9.0	4.4 ± 0.5	4.6
8	2.2 ± 0.2	2.3	6.0 ± 0.6	5.5

TABLE X. Values of $F_{(-)i}$ (%) measured from the flavor-tagged $D^0 \to K^0_S\pi^+\pi^-$ data for the equal $\Delta\delta_D$ binning derived from the Belle model. Predicted values from the *BABAR* 2008 model of $D^0 \to K^0_S\pi^+\pi^-$ are also given.

i	F_i (%)		F_{-i} (%)	
	Measured	Predicted	Measured	Predicted
1	16.5 ± 0.5	16.5	8.8 ± 0.4	8.0
2	7.7 ± 0.4	7.6	2.0 ± 0.2	1.6
3	9.8 ± 0.4	10.2	3.2 ± 0.2	2.8
4	3.0 ± 0.2	3.0	1.3 ± 0.1	1.2
5	8.0 ± 0.4	9.2	4.0 ± 0.3	4.6
6	7.1 ± 0.3	7.3	1.8 ± 0.2	1.7
7	9.9 ± 0.4	10.0	1.6 ± 0.2	1.3
8	12.4 ± 0.4	12.2	2.9 ± 0.2	2.6

values are also given. In this case the uncertainty due to the amplitude-model parameters is negligible compared to the uncertainties on the measurements. The agreement between measured and predicted values is reasonable in all cases.

We use the corrected and normalized values of the bin yields to determine $c_i^{(\prime)}$ and $s_i^{(\prime)}$. The fits to the $K^0_{S,L}\pi^+\pi^-$ and $K^0_{S,L}K^+K^-$ data are made separately. We perform the fit to $K^0_{S,L}\pi^+\pi^-$ data first because the $K^0_{S,L}K^+K^-$ fit depends upon the values of the $c_i^{(\prime)}$ and $s_i^{(\prime)}$ for $D^0 \to K^0_{S,L}\pi^+\pi^-$ decays when including $K^0_SK^+K^-$ vs. $K^0_{S,L}\pi^+\pi^-$ and $K^0_LK^+K^-$ vs. $K^0_S\pi^+\pi^-$ candidates. The fit results from the equal $\Delta\delta_D$ binning derived from the *BABAR* 2008 model are used in the fit to $K^0_{S,L}K^+K^-$ data; the $K^0_{S,L}\pi^+\pi^-$ strong-phase difference parameters are fixed to the measured values in the nominal fit, these are then varied within their errors to determine the related systematic uncertainty (Sec. VI B). In the $K^0_S\pi^+\pi^-$ analysis we obtain values of $c_i^{(\prime)}$ and $s_i^{(\prime)}$ by minimizing the log-likelihood expression

$$\begin{aligned} -2\log\mathcal{L} = & -2\sum_i \log P(M_i^{\pm}, \langle M_i^{\pm}\rangle)_{K^0_S\pi^+\pi^-,CP} \\ & - 2\sum_i \log P(M_i'^{\pm}, \langle M_i'^{\pm}\rangle)_{K^0_L\pi^+\pi^-,CP} \\ & - 2\sum_{i,j} \log P(M_{ij}, \langle M_{ij}\rangle)_{K^0_S\pi^+\pi^-,K^0_S\pi^+\pi^-} \\ & - 2\sum_{i,j} \log P(M'_{ij}, \langle M'_{ij}\rangle)_{K^0_S\pi^+\pi^-,K^0_L\pi^+\pi^-} + \chi^2. \end{aligned} \tag{23}$$

In the $K^0_SK^+K^-$ analysis we minimize the expression

$$\begin{aligned} -2\log\mathcal{L} = & -2\sum_i \log P(M_i^{\pm}, \langle M_i^{\pm}\rangle)_{K^0_SK^+K^-,CP} \\ & - 2\sum_i \log P(M_i'^{\pm}, \langle M_i'^{\pm}\rangle)_{K^0_LK^+K^-,CP} \\ & - 2\sum_{i,j} \log P(M_{ij}, \langle M_{ij}\rangle)_{K^0_SK^+K^-,K^0_SK^+K^-} \\ & - 2\sum_{i,j} \log P(M'_{ij}, \langle M'_{ij}\rangle)_{K^0_SK^+K^-,K^0_LK^+K^-} \\ & - 2\sum_{i,j} \log P(M_{ij}, \langle M_{ij}\rangle)_{K^0_SK^+K^-,K^0_S\pi^+\pi^-} \\ & - 2\sum_{i,j} \log P(M'_{ij}, \langle M'_{ij}\rangle)_{K^0_SK^+K^-,K^0_L\pi^+\pi^-} \\ & - 2\sum_{i,j} \log P(M'_{ij}, \langle M'_{ij}\rangle)_{K^0_LK^+K^-,K^0_S\pi^+\pi^-} + \chi^2. \end{aligned} \tag{24}$$

Here the expected number of CP-tagged $K^0_Sh^+h^-$ [$K^0_Lh^+h^-$] events in the i^{th} bin, $\langle M_i^{\pm}\rangle$ [$\langle M_i'^{\pm}\rangle$], is determined from Eq. (8) [Eq. (11)]. Similarly the expected number of events where both D mesons decay to $K^0_{S,L}h^+h^-$, $\langle M_{ij}\rangle$ [$\langle M'_{ij}\rangle$] is determined using Eq. (10) [Eq. (12)]. The function $P(M, \langle M\rangle)$ is the Poisson

probability of obtaining M events given a mean of $\langle M \rangle$. There is an additional χ^2 term

$$\chi^2 = \sum_i \left(\frac{c_i' - c_i - \Delta c_i}{\delta \Delta c_i} \right)^2 + \sum_i \left(\frac{s_i' - s_i - \Delta s_i}{\delta \Delta s_i} \right)^2, \quad (25)$$

which constrains the extracted c_i' (s_i') to differ within errors from c_i (s_i) by the predicted quantities Δc_i (Δs_i).

We briefly discuss the estimation of Δc_i (Δs_i) and their uncertainties. An isobar resonance model must be used to determine these constraints; we use the $D^0 \to K^0_S K^+ K^-$ and $D^0 \to K^0_S \pi^+ \pi^-$ models reported in Refs. [11,14], respectively. The intermediate resonances contributing to $D^0 \to K^0_L h^+ h^-$ model differ in two ways from those contributing to $D^0 \to K^0_S h^+ h^-$. First, DCS decays contribute with opposite sign. This can be seen by considering the $D^0 \to K^0_{S,L} h^+ h^-$ amplitudes, $\mathcal{A}$, in terms of those to the flavor eigenstates $D^0 \to K^0 h^+ h^-$ and $D^0 \to \bar{K}^0 h^+ h^-$

$$\mathcal{A}(D^0 \to K^0_S h^+ h^-) = \frac{1}{\sqrt{2}} [\mathcal{A}(D^0 \to K^0 h^+ h^-) + \mathcal{A}(D^0 \to \bar{K}^0 h^+ h^-)], \quad (26)$$

$$\mathcal{A}(D^0 \to K^0_L h^+ h^-) = \frac{1}{\sqrt{2}} [\mathcal{A}(D^0 \to K^0 h^+ h^-) - \mathcal{A}(D^0 \to \bar{K}^0 h^+ h^-)]. \quad (27)$$

The relative minus sign between the terms in $\mathcal{A}(D^0 \to K^0_L h^+ h^-)$ can be accommodated by introducing a 180° phase difference for all DCS contributions to the $D^0 \to K^0_L h^+ h^-$ model compared to the same contribution to the $D^0 \to K^0_S h^+ h^-$ model. Secondly, for CP-eigenstate amplitudes, such as $D^0 \to K^0_{S,L} \phi$, the $D^0 \to K^0_L h^+ h^-$ amplitude can be related to the $D^0 \to K^0_S h^+ h^-$ amplitude by multiplying the latter by a factor $(1 - 2re^{i\delta})$, where r is of the order $\tan^2\theta_C$ and δ can take any value. Here, θ_C is the Cabibbo angle. The origin of this factor is again related to the sign difference between DCS contributions to the $D^0 \to K^0_S h^+ h^-$ and $D^0 \to K^0_L h^+ h^-$ amplitudes, and is analogous to the mechanism which induces the difference in rates for $D \to K^0_S \pi$ and $D \to K^0_L \pi$ decay [34,38]. We determine central values of Δc_i and Δs_i by assuming $r = \tan^2\theta_C$ [23] and $\delta = 0°$. Part of the uncertainty on Δc_i and Δs_i is evaluated by randomly choosing the assumed values of r and δ 100 times, and recomputing the constraints for each set of parameters. The value of δ is assumed to have a equal probability to lie between 0° and 360° and that of r to have a Gaussian distribution of mean $\tan^2\theta_C$ and width $0.5 \times \tan^2\theta_C$. The rms of the resulting distributions of Δc_i and Δs_i are taken as the uncertainties from this source. A second source of uncertainty is related to the model choice. For the $D^0 \to K^0_S K^+ K^-$ model this is estimated by varying the isobar model parameters by their uncertainties [14], accounting for any correlations among the parameters [24], then recomputing Δc_i and Δs_i. The differences with respect to the values of the constraints computed with the nominal values of the parameters are taken as the uncertainty on Δc_i and Δs_i from this source. For $D^0 \to K^0_S \pi^+ \pi^-$ we follow Ref. [7] and consider two alternative models [10,39] to determine Δc_i and Δs_i; the largest deviation of the central value from that computed with the default model [11] is taken as a systematic uncertainty. As examples of the constraints found by this procedure, the values of Δc_i and Δs_i for the $\mathcal{N} = 3$ division of the $D^0 \to K^0_S K^+ K^-$ Dalitz plot and the optimal binning of the $D^0 \to K^0_S \pi^+ \pi^-$ Dalitz plot are given in Tables XI and XII, respectively. The size of Δc_i and Δs_i can be significant for bins dominated by either a DCS decay, such as the $K^{*+}(892)$ in bin three of the optimal $D^0 \to K^0_S \pi^+ \pi^-$ binning (Fig. 3(b)), or a neutral resonance, such as the $a^0(1450)$ in bin three of the $\mathcal{N} = 3$ division of the $D^0 \to K^0_S K^+ K^-$ Dalitz plot (Fig. 2).

The contribution of the χ^2 to the likelihood is investigated to ensure that these constraints are not leading to any significant bias. For the fits to $D^0 \to K^0_{S,L} K^+ K^-$ and $D^0 \to K^0_{S,L} \pi^+ \pi^-$ the ranges of χ^2 are 0.30 to 0.75 and 1.0 to 2.3, respectively. In addition, no individual bin contributes more than 0.9 to the total χ^2. Therefore, we conclude that the constraint is not biasing our result significantly from the values favored by the data, and is principally improving the precision of the parameters.

TABLE XI. Values of Δc_i and Δs_i constraints for the $\mathcal{N} = 3$ equal $\Delta\delta_D$ binning of the $D^0 \to K^0_S K^+ K^-$ Dalitz plot.

i	Δc_i	Δs_i
1	0.026 ± 0.014	-0.007 ± 0.023
2	0.041 ± 0.019	0.012 ± 0.010
3	-0.563 ± 0.311	0.713 ± 0.161

TABLE XII. Values of Δc_i and Δs_i constraints for the optimal $D^0 \to K^0_S \pi^+ \pi^-$ binning.

i	Δc_i	Δs_i
1	0.39 ± 0.17	0.07 ± 0.06
2	0.18 ± 0.05	0.01 ± 0.10
3	0.61 ± 0.15	0.30 ± 0.12
4	0.09 ± 0.08	0.00 ± 0.08
5	0.16 ± 0.17	0.06 ± 0.06
6	0.57 ± 0.21	-0.15 ± 0.24
7	0.03 ± 0.01	-0.04 ± 0.06
8	-0.10 ± 0.15	-0.15 ± 0.21

TABLE XIII. Measured values of c_i and s_i for the different $D^0 \to K^0_S K^+ K^-$ binnings. The first uncertainty is statistical, including that related to the Δc_i and Δs_i constraints, and the second uncertainty is systematic.

i	c_i	s_i
	$\mathcal{N} = 2$ equal $\Delta\delta_D$ bins	
1	$0.818 \pm 0.107 \pm 0.037$	$0.445 \pm 0.215 \pm 0.143$
2	$-0.746 \pm 0.083 \pm 0.035$	$0.229 \pm 0.220 \pm 0.079$
	$\mathcal{N} = 3$ equal $\Delta\delta_D$ bins	
1	$0.793 \pm 0.063 \pm 0.038$	$0.431 \pm 0.222 \pm 0.142$
2	$-0.566 \pm 0.092 \pm 0.034$	$0.413 \pm 0.234 \pm 0.094$
3	$-0.096 \pm 0.329 \pm 0.131$	$-0.461 \pm 0.432 \pm 0.175$
	$\mathcal{N} = 4$ equal $\Delta\delta_D$ bins	
1	$0.858 \pm 0.059 \pm 0.034$	$0.309 \pm 0.248 \pm 0.180$
2	$0.176 \pm 0.223 \pm 0.091$	$0.992 \pm 0.473 \pm 0.403$
3	$-0.819 \pm 0.095 \pm 0.045$	$0.307 \pm 0.267 \pm 0.201$
4	$0.376 \pm 0.329 \pm 0.157$	$-0.133 \pm 0.659 \pm 0.323$

TABLE XIV. Measured values of c'_i and s'_i for the different $D^0 \to K^0_S K^+ K^-$ binnings. The first uncertainty is statistical, including that related to the Δc_i and Δs_i constraints, and the second uncertainty is systematic.

i	c'_i	s'_i
	$\mathcal{N} = 2$ equal $\Delta\delta_D$ bins	
1	$0.839 \pm 0.108 \pm 0.073$	$0.445 \pm 0.216 \pm 0.150$
2	$-0.775 \pm 0.085 \pm 0.068$	$0.298 \pm 0.220 \pm 0.093$
	$\mathcal{N} = 3$ equal $\Delta\delta_D$ bins	
1	$0.814 \pm 0.063 \pm 0.064$	$0.422 \pm 0.222 \pm 0.143$
2	$-0.529 \pm 0.092 \pm 0.071$	$0.426 \pm 0.234 \pm 0.098$
3	$-0.583 \pm 0.349 \pm 0.197$	$0.241 \pm 0.456 \pm 0.181$
	$\mathcal{N} = 4$ equal $\Delta\delta_D$ bins	
1	$0.874 \pm 0.059 \pm 0.055$	$0.303 \pm 0.248 \pm 0.180$
2	$0.270 \pm 0.225 \pm 0.160$	$0.965 \pm 0.473 \pm 0.406$
3	$-0.810 \pm 0.096 \pm 0.060$	$0.346 \pm 0.268 \pm 0.204$
4	$-0.317 \pm 0.408 \pm 0.201$	$0.770 \pm 0.696 \pm 0.350$

The $D^0 \to K^0_{S,L} K^+ K^-$ fitting procedure has been tested using samples of signal MC events. In the validation procedure, the number of events for each tag is assumed to follow a Poisson distribution about the mean expectation, while the ratio between double-tagged events and single-tagged events is computed as $\mathcal{B}_{K^0_S K^+ K^-}/2$, ignoring quantum correlations. The means of the fitted c_i and s_i distributions exhibit small, but statistically significant, biases due to the assumptions made in the fit. The systematic uncertainty we associate to the bias is described in Sec. VI B.

The parameters that result from fits to the $D^0 \to K^0_{S,L} K^+ K^-$ data divided into $\mathcal{N} = 2$, $\mathcal{N} = 3$, and $\mathcal{N} = 4$ equal $\Delta\delta_D$ bins are given in Tables XIII and XIV. The statistical uncertainty on the parameters includes that related to the Δc_i and Δs_i constraints. The statistical correlations among the parameters for the $\mathcal{N} = 3$ equal $\Delta\delta_D$ binning are shown in Table XV. The other statistical correlations are given in Ref. [40].

Tables XVI and XVII give the fit results for the $D^0 \to K^0_{S,L} \pi^+ \pi^-$ data divided according to the four different binnings. The statistical correlation matrices for each binning are given in Ref. [40].

VI. SYSTEMATIC UNCERTAINTIES

The systematic uncertainties on the measured values of $c_i^{(\prime)}$ and $s_i^{(\prime)}$ come from a variety of sources. Tables XVIII and XIX give examples of the individual sources of uncertainty for the $\mathcal{N} = 3$ equal $\Delta\delta_D$ binning of the $D^0 \to K^0_S K^+ K^-$ Dalitz plot and the equal $\Delta\delta_D$ binning of the $D^0 \to K^0_S \pi^+ \pi^-$ Dalitz plot, respectively. The breakdown of the systematic uncertainty is similar for the other binnings considered for $D^0 \to K^0_S K^+ K^-$ and $D^0 \to K^0_S \pi^+ \pi^-$ data. Many of the systematic uncertainties are from common sources for the two final states; these are described in Sec. VI A. The sources of uncertainty considered exclusively for the $D^0 \to K^0_S K^+ K^-$ analysis, or those that

TABLE XV. Statistical correlations (%) among the parameters for $\mathcal{N} = 3$ equal $\Delta\delta_D$ binning of the $D^0 \to K^0_S K^+ K^-$ Dalitz plot.

	c_2	c_3	s_1	s_2	s_3	c'_1	c'_2	c'_3	s'_1	s'_2	s'_3
c_1	0.6	−2.9	−1.3	−0.6	−0.2	97.6	0.6	−2.1	−1.3	−0.6	−0.1
c_2		0.8	1.1	3.2	−0.0	0.6	98.0	0.4	1.1	3.2	−0.0
c_3			−0.3	0.2	2.5	−2.8	0.8	66.4	−0.3	0.2	2.4
s_1				−2.0	6.1	−1.3	1.1	−0.1	99.4	−2.0	5.8
s_2					−3.3	−0.5	3.2	0.1	−1.9	99.9	−3.0
s_3						−0.2	−0.0	2.2	6.1	−3.3	93.7
c'_1							0.6	−2.0	−1.3	−0.5	−0.1
c'_2								0.4	1.1	3.2	−0.0
c'_3									−0.1	0.1	2.2
s'_1										−1.9	5.8
s'_2											−3.0

TABLE XVI. Measured values of c_i and s_i for the different $D^0 \to K^0_S\pi^+\pi^-$ binnings. The first uncertainty is statistical, including that related to the Δc_i and Δs_i constraints, and the second uncertainty is systematic.

	Optimal		Equal $\Delta\delta_D$ *BABAR* 2008	
i	c_i	s_i	c_i	s_i
1	$-0.009 \pm 0.088 \pm 0.094$	$-0.438 \pm 0.184 \pm 0.045$	$0.655 \pm 0.036 \pm 0.042$	$-0.025 \pm 0.098 \pm 0.043$
2	$0.900 \pm 0.106 \pm 0.082$	$-0.490 \pm 0.295 \pm 0.261$	$0.511 \pm 0.068 \pm 0.063$	$0.141 \pm 0.183 \pm 0.066$
3	$0.292 \pm 0.168 \pm 0.139$	$-1.243 \pm 0.341 \pm 0.123$	$0.024 \pm 0.140 \pm 0.080$	$1.111 \pm 0.131 \pm 0.044$
4	$-0.890 \pm 0.041 \pm 0.044$	$-0.119 \pm 0.141 \pm 0.038$	$-0.569 \pm 0.118 \pm 0.098$	$0.328 \pm 0.202 \pm 0.072$
5	$-0.208 \pm 0.085 \pm 0.080$	$0.853 \pm 0.123 \pm 0.035$	$-0.903 \pm 0.045 \pm 0.042$	$-0.181 \pm 0.131 \pm 0.026$
6	$0.258 \pm 0.155 \pm 0.108$	$0.984 \pm 0.357 \pm 0.165$	$-0.616 \pm 0.103 \pm 0.072$	$-0.520 \pm 0.196 \pm 0.059$
7	$0.869 \pm 0.034 \pm 0.033$	$-0.041 \pm 0.132 \pm 0.034$	$0.100 \pm 0.106 \pm 0.124$	$-1.129 \pm 0.120 \pm 0.096$
8	$0.798 \pm 0.070 \pm 0.047$	$-0.107 \pm 0.240 \pm 0.080$	$0.422 \pm 0.069 \pm 0.075$	$-0.350 \pm 0.151 \pm 0.045$
	Modified optimal		Equal $\Delta\delta_D$ Belle	
i	c_i	s_i	c_i	s_i
1	$-0.216 \pm 0.104 \pm 0.088$	$-0.399 \pm 0.204 \pm 0.049$	$0.710 \pm 0.034 \pm 0.038$	$-0.013 \pm 0.097 \pm 0.031$
2	$0.827 \pm 0.060 \pm 0.053$	$-0.031 \pm 0.172 \pm 0.084$	$0.481 \pm 0.080 \pm 0.070$	$-0.147 \pm 0.177 \pm 0.107$
3	$0.101 \pm 0.085 \pm 0.118$	$-0.558 \pm 0.161 \pm 0.070$	$0.008 \pm 0.080 \pm 0.087$	$0.938 \pm 0.120 \pm 0.047$
4	$-0.955 \pm 0.038 \pm 0.034$	$-0.204 \pm 0.137 \pm 0.055$	$-0.757 \pm 0.099 \pm 0.065$	$0.386 \pm 0.208 \pm 0.067$
5	$-0.522 \pm 0.095 \pm 0.079$	$0.911 \pm 0.130 \pm 0.067$	$-0.884 \pm 0.056 \pm 0.054$	$-0.162 \pm 0.130 \pm 0.041$
6	$0.291 \pm 0.102 \pm 0.075$	$1.030 \pm 0.196 \pm 0.065$	$-0.462 \pm 0.100 \pm 0.082$	$-0.616 \pm 0.188 \pm 0.052$
7	$0.682 \pm 0.051 \pm 0.047$	$-0.037 \pm 0.146 \pm 0.029$	$0.106 \pm 0.105 \pm 0.100$	$-1.063 \pm 0.174 \pm 0.066$
8	$0.724 \pm 0.071 \pm 0.044$	$-0.180 \pm 0.194 \pm 0.050$	$0.365 \pm 0.071 \pm 0.078$	$-0.179 \pm 0.166 \pm 0.048$

TABLE XVII. Measured values of c'_i and s'_i for the different $D^0 \to K^0_S\pi^+\pi^-$ binnings. The first uncertainty is statistical, including that related to the Δc_i and Δs_i constraints, and the second uncertainty is systematic.

	Optimal		Equal $\Delta\delta_D$ *BABAR* 2008	
i	c'_i	s'_i	c'_i	s'_i
1	$0.470 \pm 0.096 \pm 0.102$	$-0.363 \pm 0.185 \pm 0.191$	$0.768 \pm 0.038 \pm 0.051$	$-0.079 \pm 0.095 \pm 0.108$
2	$1.073 \pm 0.102 \pm 0.126$	$-0.501 \pm 0.297 \pm 0.397$	$0.679 \pm 0.067 \pm 0.090$	$0.080 \pm 0.183 \pm 0.196$
3	$0.869 \pm 0.142 \pm 0.165$	$-0.890 \pm 0.329 \pm 0.352$	$0.278 \pm 0.106 \pm 0.112$	$1.090 \pm 0.106 \pm 0.119$
4	$-0.786 \pm 0.047 \pm 0.052$	$-0.137 \pm 0.154 \pm 0.159$	$-0.446 \pm 0.116 \pm 0.128$	$0.455 \pm 0.219 \pm 0.235$
5	$-0.139 \pm 0.089 \pm 0.093$	$0.921 \pm 0.126 \pm 0.132$	$-0.824 \pm 0.051 \pm 0.056$	$-0.194 \pm 0.136 \pm 0.140$
6	$0.654 \pm 0.135 \pm 0.152$	$0.832 \pm 0.326 \pm 0.362$	$-0.240 \pm 0.116 \pm 0.123$	$-0.557 \pm 0.201 \pm 0.211$
7	$0.901 \pm 0.034 \pm 0.047$	$-0.076 \pm 0.132 \pm 0.137$	$0.480 \pm 0.106 \pm 0.113$	$-0.975 \pm 0.104 \pm 0.141$
8	$0.817 \pm 0.090 \pm 0.095$	$-0.157 \pm 0.281 \pm 0.306$	$0.708 \pm 0.066 \pm 0.083$	$-0.285 \pm 0.150 \pm 0.158$
	Modified optimal		Equal $\Delta\delta_D$ Belle	
i	c'_i	s'_i	c'_i	s'_i
1	$-0.049 \pm 0.108 \pm 0.125$	$-0.386 \pm 0.218 \pm 0.226$	$0.817 \pm 0.035 \pm 0.048$	$-0.070 \pm 0.095 \pm 0.103$
2	$0.935 \pm 0.056 \pm 0.072$	$-0.028 \pm 0.168 \pm 0.191$	$0.668 \pm 0.079 \pm 0.104$	$-0.219 \pm 0.176 \pm 0.209$
3	$0.614 \pm 0.082 \pm 0.089$	$-0.398 \pm 0.160 \pm 0.175$	$0.197 \pm 0.082 \pm 0.090$	$0.935 \pm 0.117 \pm 0.130$
4	$-0.876 \pm 0.047 \pm 0.051$	$-0.249 \pm 0.139 \pm 0.149$	$-0.592 \pm 0.117 \pm 0.125$	$0.520 \pm 0.254 \pm 0.268$
5	$-0.357 \pm 0.094 \pm 0.100$	$0.980 \pm 0.131 \pm 0.151$	$-0.720 \pm 0.056 \pm 0.062$	$-0.192 \pm 0.135 \pm 0.142$
6	$0.584 \pm 0.094 \pm 0.103$	$0.963 \pm 0.200 \pm 0.214$	$-0.121 \pm 0.108 \pm 0.117$	$-0.630 \pm 0.194 \pm 0.203$
7	$0.789 \pm 0.058 \pm 0.070$	$-0.091 \pm 0.145 \pm 0.149$	$0.426 \pm 0.104 \pm 0.113$	$-0.922 \pm 0.179 \pm 0.194$
8	$0.717 \pm 0.080 \pm 0.089$	$-0.219 \pm 0.201 \pm 0.209$	$0.641 \pm 0.071 \pm 0.089$	$-0.095 \pm 0.164 \pm 0.172$

are evaluated in a significantly different fashion than $D^0 \to K^0_S\pi^+\pi^-$, are described in Sec. VI B. A discussion of the uncertainties related to the acceptance and background to the $D^0 \to K^0_S\pi^+\pi^-$ analysis are given in Sec. VI C. A brief discussion of the uncertainty related to the constraints Δc_i and Δs_i is given in Sec. VI D.

A. Common systematic uncertainties

The statistical uncertainties on the measurements of $K^{(\prime)}_i$ using flavor and pseudoflavor tagged events are not included in the fit to determine c_i, s_i, c'_i, and s'_i. Even though there are significantly more flavor and pseudoflavor tagged events than the CP-tagged or $K^0_{S,L}h^+h^-$ vs. $K^0_S h^+h^-$

TABLE XVIII. Statistical and systematic uncertainties on c_i and s_i determined for the $\mathcal{N} = 3$ equal $\Delta\delta_D$ binning of $D^0 \to K^0_S K^+ K^-$ data.

Uncertainty	c_1	c_2	c_3	s_1	s_2	s_3
(Pseudo)flavor statistics	0.005	0.007	0.055	0.015	0.013	0.039
Momentum resolution	0.002	0.004	0.012	0.018	0.025	0.032
Mode-to-mode normalization	0.004	0.008	0.017	0.001	0.010	0.004
Multiple-candidate selection	0.004	0.003	0.015	0.004	0.008	0.002
DCS correction	0.001	0.001	0.003	0.002	0.005	0.002
$K^0_{S,L}\pi^+\pi^-$ $(c_i^{(\prime)}, s_i^{(\prime)})$	0.006	0.011	0.036	0.132	0.063	0.135
Fitter assumptions	0.008	0.001	0.013	0.013	0.003	0.043
MC statistics for determining **U**	0.005	0.007	0.057	0.024	0.051	0.048
Parameterization of non-K^0_L final-state background	0.001	0.001	0.006	0.000	0.008	0.003
Parameterization of K^0_L final -state background	0.034	0.020	0.061	0.038	0.015	0.071
Background Dalitz-space distribution	0.006	0.015	0.062	0.005	0.029	0.022
Assumed background $\mathcal{B}$	0.004	0.014	0.032	0.001	0.007	0.009
Total systematic	0.038	0.034	0.131	0.142	0.094	0.175
Statistical plus $K^0_L K^+ K^-$ model	0.063	0.092	0.329	0.222	0.234	0.432
$K^0_L K^+ K^-$ model alone	0.000	0.000	0.136	0.007	0.000	0.039
Total	0.073	0.098	0.354	0.264	0.252	0.466

TABLE XIX. Statistical and systematic uncertainties on c_i and s_i determined for the equal binning of $D^0 \to K^0_S\pi^+\pi^-$ data.

Uncertainty	c_1	c_2	c_3	c_4	c_5	c_6	c_7	c_8
(Pseudo)flavor statistics	0.005	0.010	0.009	0.012	0.005	0.013	0.013	0.010
Momentum resolution	0.007	0.013	0.016	0.022	0.007	0.021	0.021	0.016
Mode-to-mode normalization	0.007	0.010	0.015	0.018	0.008	0.014	0.024	0.013
Multiple-candidate selection	0.014	0.014	0.024	0.022	0.008	0.014	0.032	0.019
DCS correction	0.001	0.002	0.001	0.002	0.002	0.004	0.003	0.003
Dalitz-plot acceptance	0.004	0.005	0.009	0.008	0.006	0.009	0.011	0.006
Tag-side background	0.024	0.032	0.049	0.059	0.027	0.046	0.079	0.046
$K^0_S\pi^+\pi^-$ signal-side background	0.014	0.020	0.028	0.034	0.016	0.025	0.049	0.026
$K^0_L\pi^+\pi^-$ signal-side background	0.017	0.035	0.032	0.047	0.017	0.022	0.046	0.032
Continuum background	0.020	0.026	0.031	0.038	0.017	0.029	0.049	0.031
Total systematic	0.042	0.063	0.080	0.098	0.042	0.072	0.124	0.075
Statistical plus $K^0_L\pi^+\pi^-$ model	0.036	0.068	0.088	0.119	0.045	0.102	0.105	0.069
$K^0_L\pi^+\pi^-$ model alone	0.013	0.018	0.039	0.068	0.024	0.040	0.068	0.034
Total	0.056	0.093	0.119	0.154	0.062	0.125	0.163	0.102
Uncertainty	s_1	s_2	s_3	s_4	s_5	s_6	s_7	s_8
(Pseudo)flavor statistics	0.008	0.014	0.022	0.021	0.012	0.019	0.042	0.017
Momentum resolution	0.021	0.037	0.030	0.041	0.019	0.041	0.039	0.030
Mode-to-mode normalization	0.001	0.000	0.002	0.002	0.001	0.002	0.001	0.001
Multiple-candidate selection	0.016	0.007	0.008	0.010	0.004	0.007	0.010	0.007
DCS correction	0.004	0.003	0.011	0.004	0.001	0.007	0.016	0.008
Dalitz-plot acceptance	0.006	0.004	0.005	0.005	0.005	0.004	0.007	0.004
Tag-side background	0.004	0.001	0.007	0.005	0.002	0.003	0.004	0.005
$K^0_S\pi^+\pi^-$ signal-side background	0.002	0.005	0.005	0.005	0.005	0.008	0.003	0.007
$K^0_L\pi^+\pi^-$ signal-side background	0.031	0.051	0.016	0.054	0.010	0.035	0.074	0.024
Continuum background	0.003	0.004	0.006	0.006	0.001	0.002	0.006	0.004
Total systematic	0.043	0.066	0.044	0.072	0.026	0.059	0.096	0.045
Statistical plus $K^0_L\pi^+\pi^-$ model	0.098	0.182	0.086	0.202	0.131	0.197	0.131	0.150
$K^0_L\pi^+\pi^-$ model alone	0.037	0.038	0.000	0.000	0.030	0.006	0.000	0.025
Total	0.106	0.193	0.097	0.214	0.133	0.206	0.162	0.157

events, there is a non-negligible uncertainty related to the limited statistics of these samples. Each input is varied separately by its uncertainty and the fits are repeated. The differences with respect to the nominal fit are added quadratically to attain the systematic uncertainty.

The unusual shape of the bins, particularly those with narrow regions, allows the possibility that a mismodeling of the invariant-mass resolution leads to an incorrect description of the bin-to-bin migration. In the analysis of $K^0_S K^+ K^-$ the invariant-mass resolution is estimated from the width of the ϕ peak in data and MC. The difference is compatible with zero but it is conservatively assumed that the MC underestimates the resolution by up to 1 standard deviation of the measured difference. The invariant masses in the signal MC simulation sample are smeared by this difference and then fit to extract c_i and s_i. This procedure is repeated many times and the resulting distributions of c_i and s_i returned from the fits are used to determine the systematic uncertainty on these parameters due to resolution. The uncertainty related to the invariant-mass resolution in $D^0 \to K^0_S \pi^+ \pi^-$ events is evaluated in similar fashion with the momentum of the charged tracks smeared by the CLEO-c resolution as in the previous analysis [7].

The mode-to-mode normalization in the fitter is performed either using the measured branching fractions of the modes combined with $N_{D^0\bar{D}^0}$, or the measured ST yields. For the $K^0_S K^+ K^-$ analysis the former method is used apart from normalizing the $K^0_{S,L} K^+ K^-$ *vs.* $K^0_S \pi^+ \pi^-$ yields, where the pseudoflavor ST yields are used. In the $K^0_S \pi^+ \pi^-$ analysis the ST yields are used apart from the two final states that contain unreconstructed particles in the tag candidate ($K^- e^+ \nu$ and $K^0_L \pi^0$). In addition, previous investigations [32] have determined that there are small differences in the particle-reconstruction efficiency between data and the MC. These differences lead to systematic uncertainties, and in some cases corrections, for final states in which $K^0_{S,L} h^+ h^-$ is normalized using the branching fraction and the $N_{D^0\bar{D}^0}$; when using ST yields to normalize, these corrections and uncertainties cancel. The reconstruction efficiency of each final state containing a π^0 or an η meson must be corrected. The DT efficiency has an uncertainty for each final-state particle reconstructed due to the MC modeling. These uncertainties are: 0.3% per π^+, 0.6% per K^+, 1.3% per π^0, 4% per η, 0.9% per K^0_S, and 3% per K^0_L candidates. If a final state contains two particles of the same type the uncertainty on each identical particle is treated as fully correlated. The uncertainties on the ST yields, branching fractions, $N_{D^0\bar{D}^0}$, and particle reconstruction efficiency are used to estimate the systematic uncertainty from the mode-to-mode normalization method.

The method used to select the best candidate in an event when there are multiple candidates can introduce a bias. To estimate the systematic uncertainty related to the multiple-candidate selection the simulation is used to determine how often the wrong candidate is selected. This information is used to derive corrections to the yields. The difference between the c_i and s_i parameters fit with and without this correction applied is taken as the systematic uncertainty due to the multiple-candidate selection.

The use of $D^0 \to K^- \pi^+$, $D^0 \to K^- \pi^+ \pi^0$ and $D^0 \to K^- \pi^+ \pi^+ \pi^-$ pseudoflavor tags has a systematic uncertainty from the values of the three amplitude ratios r_D, the three strong-phase differences δ_D, and the two coherence parameters required to estimate the corrections from DCS contamination. The uncertainty is estimated by performing the fit to c_i and s_i for each parameter shifted by plus or minus the uncertainties given in Table V. The largest change in each c_i and s_i, from either the positive or negative shift in the parameter, is taken as the symmetric systematic uncertainty on the parameter. The total uncertainty is the sum in quadrature of the individual parameters. The uncertainties on the strong-phase differences and coherence parameters dominate the total uncertainty from this source.

B. $K^0_S K^+ K^-$ specific systematic uncertainties

There are specific systematic uncertainties related to the $K^0_S K^+ K^-$ analysis: the strong-phase parameters of the $K^0_S \pi^+ \pi^-$ events in the analysis, assumptions in the fitting procedure, the determination of the migration matrix, and the background assumptions. The use of $K^0_{S,L} K^+ K^-$ vs. $K^0_S \pi^+ \pi^-$ and $K^0_S K^+ K^-$ vs. $K^0_L \pi^+ \pi^-$ events introduces a dependence on the values of $c_i^{(\prime)}$ and $s_i^{(\prime)}$ for $D^0 \to K^0_{L,S} \pi^+ \pi^-$ derived from the equal $\Delta\delta_D$ binning reported in this paper. The nominal fit has the values of $c_i^{(\prime)}$ and $s_i^{(\prime)}$ fixed to the central values. To determine the systematic uncertainty the input values are smeared by their uncertainties and the fit repeated. This is done many times and the width of the distribution of c_i and s_i parameters returned for the particular $K^0_S K^+ K^-$ binning is taken as the systematic uncertainty from this source.

The $K^0_S K^+ K^-$ fit was tested on samples of signal MC data. It was found that there were small but statistically significant biases in the central values of c_i and s_i returned by the fitter. These biases are likely to be consequences of the assumptions used in the fit such as the finite granularity of the Dalitz plot bit-map and DT branching fractions not being corrected for quantum correlations. The whole bias is conservatively taken as an additional source of systematic and is found to be significantly smaller than both the statistical uncertainty and the dominant sources of systematic uncertainty. (No such bias is observed in the validation of the $K^0_S \pi^+ \pi^-$ fitter [7]; therefore, no uncertainty is attributed to fitter bias in that analysis.)

The elements of the migration matrices, **U**, are determined from MC samples of signal events. The resulting statistical uncertainty on the elements due to the finite sample size introduces a systematic error on the $c^{(\prime)}$ and $s^{(\prime)}$ parameters. The uncertainty is determined by smearing

the elements by their statistical error accounting for correlations. Then the fit is repeated with the new migration matrices. The procedure is repeated many times and the width of the resulting distribution of $c^{(\prime)}$ and $s^{(\prime)}$ is taken as the systematic uncertainty from this source.

The background parametrization contains several sources of systematic uncertainties. For final states without a K^0_L meson the limited statistics of the generic MC sample, which is used to determine the peaking backgrounds, leads to an uncertainty in the background parameterization. For K^0_L there are also uncertainties arising from the ratios of signal-to-background events in the signal region, as well as the high and low missing-mass sidebands, which are obtained from the simulation. This fact, combined with the more significant backgrounds in the modes containing a K^0_L meson, leads to a larger uncertainty due to MC parameterizations of the background for final states that include a K^0_L meson. We vary these parameters by their uncertainties, repeat the fit then compare the result to the nominal fit to determine the uncertainty from this source.

The assumptions about the distribution of the background events over Dalitz space are also varied to determine a systematic uncertainty. In the nominal fits the distribution for each background type is either assumed to be uniform or to follow the $K^0_S K^+ K^-$ signal distribution. We assign a systematic uncertainty to these assumptions by randomly choosing the fraction of the background that is uniformly distributed for each source of background; the remainder of that background component is then assumed to follow the distribution of $D^0 \to K^0_S K^+ K^-$ events. The fraction is assumed to have equal probability of taking any value between 0 and 1. Then the fit is performed with these assumptions about the Dalitz plot distribution. This procedure is repeated many times and the resulting distributions of c_i and s_i are used to determine the systematic uncertainty related to the assumed distribution of background over the Dalitz space.

The final source of uncertainty is related to the branching fractions, $\mathcal{B}$, assumed when generating the generic MC samples. For modes that contribute background we vary the branching fraction by the uncertainty reported in Ref. [23] and repeat the fit to determine the systematic uncertainty on $c_i^{(\prime)}$ and $s_i^{(\prime)}$.

C. Uncertainties related to the acceptance and backgrounds in the $K^0_S \pi^+ \pi^-$ analysis

The sources of uncertainty related to the acceptance and background in the $K^0_S \pi^+ \pi^-$ analysis are identical to those considered in Ref. [7]. In addition, the same evaluation procedures are adopted, which we briefly outline here.

Any difference in the relative efficiency over the Dalitz space can bias the results. In the nominal fit the Dalitz plot acceptance is taken from simulation. To account for any difference between data and simulation, the relative efficiency is smeared in each bin by 2%, which is the spread of efficiencies observed in simulation, and a sample of signal MC is fit with the new efficiencies. This procedure is repeated many times and the resulting distributions of c_i and s_i returned from the fits are used to determine the systematic uncertainty on these parameters due to modeling the acceptance. (The relative variation of efficiency is an order of magnitude greater for $D^0 \to K^0_S K^+ K^-$ due to the momentum dependence of the charged kaon detection efficiency. Therefore, adopting a similar approach would be too conservative. However, the observed relative variation in efficiency from the momentum and migration matrix smearing for $D^0 \to K^0_S K^+ K^-$ is around 5%, which is greater than the fluctuations assumed for $D^0 \to K^0_S \pi^+ \pi^-$.)

Tag-side background yields are evaluated mode-by-mode from sidebands. The distribution over Dalitz space is assumed to follow that found in the simulation. The fits are repeated assuming the background events are distributed uniformly over Dalitz space. The difference between the fits is taken as the systematic uncertainty.

The nominal fit ignores background in the signal $K^0_S \pi^+ \pi^-$ Dalitz space. The level of background estimated from K^0_S mass sidebands is 1.9% [7]. The background distribution is estimated from MC samples that include the effect of quantum correlations and the fit is repeated with the background subtracted. The difference between the nominal fit and the fit including background is taken as the systematic uncertainty due to signal-side $K^0_S \pi^+ \pi^-$ background.

The nominal fit assumes the signal-side $K^0_L \pi^+ \pi^-$ background is distributed over Dalitz space following the distribution observed in the K^0_L mass sidebands. The fit is repeated assuming the background is distributed uniformly over Dalitz space and the difference in the parameter values taken as the systematic uncertainty.

The continuum background is only significant in $K^0_L \pi^+ \pi^-$ events tagged by $K^0_S \pi^0$ and $K^0_S \pi^+ \pi^-$ decays. The distribution of the continuum events over Dalitz space is taken from the simulation. The fit is repeated with the continuum events distributed uniformly over Dalitz space. The difference between the fitted values of c_i and s_i between the two distribution assumptions is taken as the systematic uncertainty related to the continuum background.

D. The $K^0_L h^+ h^-$ model uncertainty

The statistical uncertainty returned by the fit includes a contribution that is related to the assigned uncertainties on Δc_i and Δs_i present in the χ^2 term of Eqs. (23) and (24). In order to isolate this contribution the fit can be repeated fixing Δc_i and Δs_i, then the variance related to the constraint is the difference between the variances returned by the fit with fixed or constrained values of Δc_i and Δs_i. However, due to the variations in the central values of s_i and c_i and the non-Gaussian behavior of the parameters near the edges of the physical region ($c_i^2 + s_i^2 < 1$), the covariance matrix related to the uncertainty on the constraint is found to give

unphysical values in some cases; these are either negative diagonal elements or off-diagonal terms that correspond to correlations greater than one or less than minus one. Therefore, we present the statistical covariance matrix from the constrained fit and the systematic covariance matrix from all other sources of systematic uncertainty.

To indicate that the size of the uncertainties related to Δc_i and Δs_i are not dominant, the estimated values are given in Tables XVIII and XIX. The procedure outlined above is used to estimate these $K^0_L h^+ h^-$ model uncertainties. In cases where the diagonal elements of the covariance matrix are negative the uncertainty is set to zero.

E. Summary of systematic uncertainties

In both the $K^0_S h^+ h^-$ analyses the largest sources of uncertainty is usually the background parameterization. In some bins there are significant contributions from the momentum resolution, flavor-tag statistics, and the knowledge of strong-phase parameters. The determinations of c_i have a systematic uncertainty comparable in size to the statistical uncertainty whereas for s_i measurements the statistical uncertainty dominates. Correlation matrices for the systematic uncertainties associated with the different binnings are given in Ref. [40].

VII. FINAL RESULTS, IMPACT ON γ/ϕ_3 AND CP CONTENT OF $D^0 \to K^0_S K^+ K^-$

Section VII A presents the final results for $c_i^{(\prime)}$ and $s_i^{(\prime)}$, along with comparison of the measured values with the amplitude model predictions. The impact of the c_i and s_i results on the determination of γ/ϕ_3 is discussed in Sec. VII B. In addition, results for the CP-odd fraction,

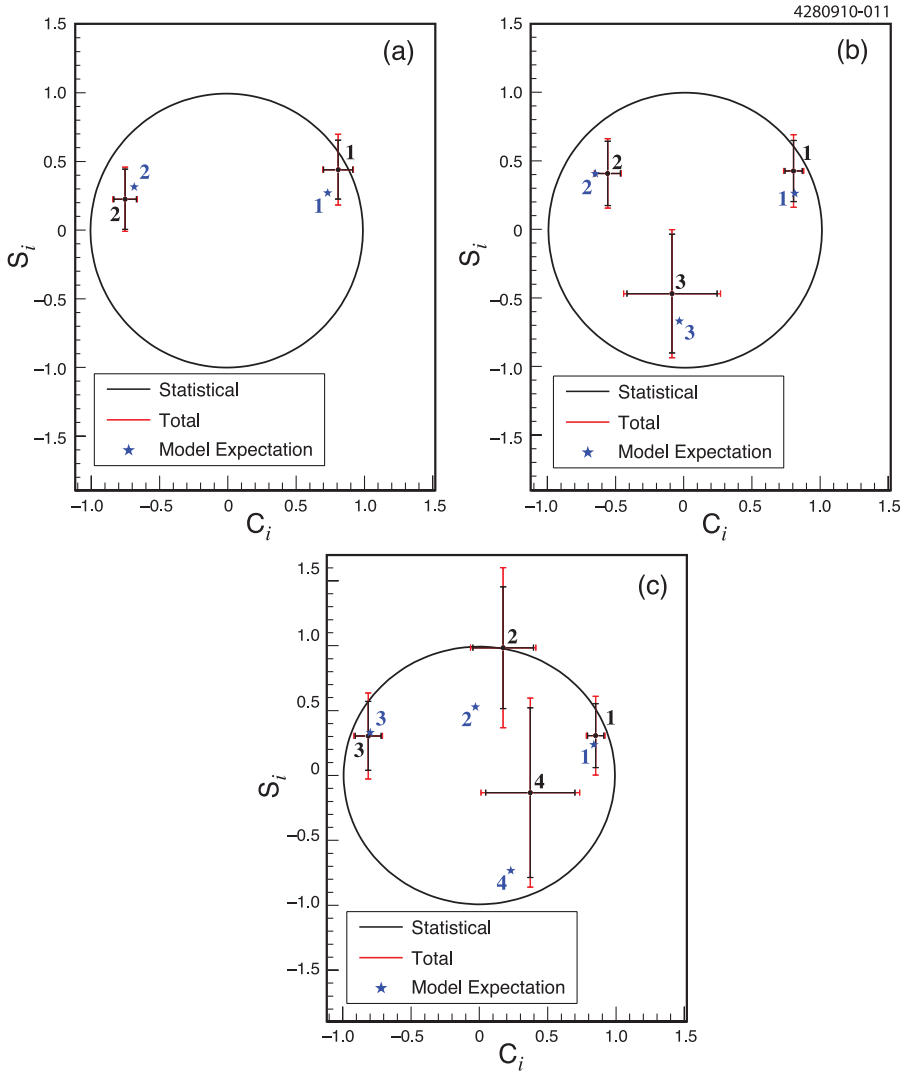

FIG. 13 (color online). Measured values of c_i and s_i for $D^0 \to K^0_S K^+ K^-$ data divided into (a) $\mathcal{N} = 2$, (b) $\mathcal{N} = 3$, and (c) $\mathcal{N} = 4$ equal $\Delta\delta_D$ bins. The expected values calculated from the *BABAR* 2010 model are indicated by the stars. The circle indicates the boundary of the physical region $c_i^2 + s_i^2 = 1$.

TABLE XX. Values of χ^2 per DOF and the corresponding probability for comparison of measured values of c_i and s_i with those predicted by the *BABAR* 2010 and *BABAR* 2008 models for $D^0 \to K^0_S K^+ K^-$ and $D^0 \to K^0_S \pi^+ \pi^-$, respectively.

Binning	χ^2/DOF	Probability
$D^0 \to K^0_S K^+ K^-$		
$\mathcal{N} = 2$ equal $\Delta\delta_D$	1.7/4	79%
$\mathcal{N} = 3$ equal $\Delta\delta_D$	1.4/6	96%
$\mathcal{N} = 4$ equal $\Delta\delta_D$	2.2/8	98%
$D^0 \to K^0_S \pi^+ \pi^-$		
Optimal	15.5/16	49%
BABAR 2008 equal $\Delta\delta_D$	25.3/16	6.5%
Modified optimal	13.8/16	61%
Belle	26.8/16	4.4%

$\mathcal{F}_-$, of $D^0 \to K^0_S K^+ K^-$ decays in the region of the ϕ resonance are presented in Sec. VII C.

A. Final results for $c_i^{(\prime)}$ and $s_i^{(\prime)}$

The measured values of c_i and s_i are shown in Figs. 13 and 14 for $D^0 \to K^0_S K^+ K^-$ and $D^0 \to K^0_S \pi^+ \pi^-$, respectively. Also, shown are the expectations from the *BABAR* 2010 model and *BABAR* 2008 model for $D^0 \to K^0_S K^+ K^-$ and $D^0 \to K^0_S \pi^+ \pi^-$, respectively. To test the compatibility of our results with the predictions of the models we compute

$$\chi^2 = (\mathbf{P} - \mathbf{P}^{\text{model}})^T \mathbf{V}^{-1} (\mathbf{P} - \mathbf{P}^{\text{model}}), \tag{28}$$

where $\mathbf{P}$ is a vector of the $2\mathcal{N}$ measured values of c_i and s_i, $\mathbf{P}^{\text{model}}$ is the equivalent vector of c_i and s_i values predicted by the models, and $\mathbf{V}$ is the $2\mathcal{N} \times 2\mathcal{N}$ combined statistical and systematic covariance matrix. Table XX gives the values of the χ^2 and the corresponding probabilities. In the case of $D^0 \to K^0_S K^+ K^-$ the agreement between measured and predicted values of c_i and s_i is good for all binnings. For $D^0 \to K^0_S \pi^+ \pi^-$ the compatibility of the model predictions with the optimal and modified-optimal binning results is very good; the compatibility of the models with the *BABAR* 2008 and Belle model equal $\Delta\delta_D$ binnings is reasonable. The compatibility with the predictions from the Belle model is also tested and is found to be reasonable.

B. Impact of c_i and s_i measurements on determining γ/ϕ_3

Our measurements of c_i and s_i have two consequences on the determination of γ/ϕ_3 from a model-independent analysis:

(i) the uncertainties on c_i and s_i will result in a systematic uncertainty on the determination of γ/ϕ_3, and
(ii) the choice of binning affects the statistical precision of a γ/ϕ_3 measurement.

Therefore, we investigate the impact on future γ/ϕ_3 measurements using a simplified MC simulation of B-decay data on which we perform the model-independent determination of γ/ϕ_3 [5]. The number of B^- decays in a given bin of Dalitz space is dependent on c_i, s_i, r_B, δ_B, γ/ϕ_3, and normalization parameters. The input values used for r_B, δ_B, and γ/ϕ_3 are 0.1, 130°, and 60°, respectively, which are consistent with current measurements [2,3]. The values of $K_{(-)i}$ are those predicted by the respective models. The yield in each bin is generated randomly according to the input values, and a χ^2 fit between the observed and expected events in each bin is performed to extract the value of γ/ϕ_3.

To determine the systematic uncertainty in future γ/ϕ_3 measurements due to the uncertainty in the measured strong phases we generate samples of 5×10^6 signal events using the measured values of c_i and s_i. The samples are then fit using the measured central values smeared according to their uncertainties, with the correlation between parameters taken into account. The large number of signal events means that the width of distribution of fitted γ/ϕ_3 gives the systematic uncertainty due to the uncertainty in c_i and s_i, as the intrinsic width due to the statistical fluctuations for 5×10^6 events is negligible in comparison.

For the $\tilde{D}^0 \to K^0_S K^+ K^-$ mode, the induced uncertainty on γ/ϕ_3 due to the total uncertainties on c_i and s_i is evaluated from the rms of γ distribution returned by the fits to the simulated experiments. The induced uncertainty is 3.9°, 3.2°, and 3.9° for two, three, and four bins, respectively. The larger uncertainty for four bins reflects the limited statistics available to determine the parameters in each bin. It can be noted that there is only a limited improvement in the statistical sensitivity to γ/ϕ_3 by increasing the number of bins, since most of the sensitivity is due to the dominant resonances, $K^0_S\phi$ and $K^0_S a^0(980)$, which lie in the same region of the Dalitz plot close to the $m_{K^+K^-}$ threshold.

For the $\tilde{D}^0 \to K^0_S \pi^+ \pi^-$ case we find the uncertainty on γ/ϕ_3 related to the uncertainties on c_i and s_i in a similar manner. The uncertainty varies significantly between the different binnings. For the equal $\Delta\delta_D$ binning derived from the *BABAR* 2008 model, we find an induced uncertainty of 2.0°, whereas for the optimal binning it is 3.9°. These variations reflect the limited statistics available with which to determine c_i and s_i in some of the optimal bins; these are the same bins that lead to the reduced statistical performance in determining γ from the optimal binning in the presence of background. This is further emphasized by the expected uncertainty on γ/ϕ_3 from the modified-optimal binning results being 2.1°. The values of c_i and s_i measured for the equal $\Delta\delta_D$ binning derived from the Belle model lead to a 1.7° uncertainty on γ/ϕ_3. In all cases the error on the predicted uncertainty is less than 0.1° and the contribution of the systematic uncertainties on c_i

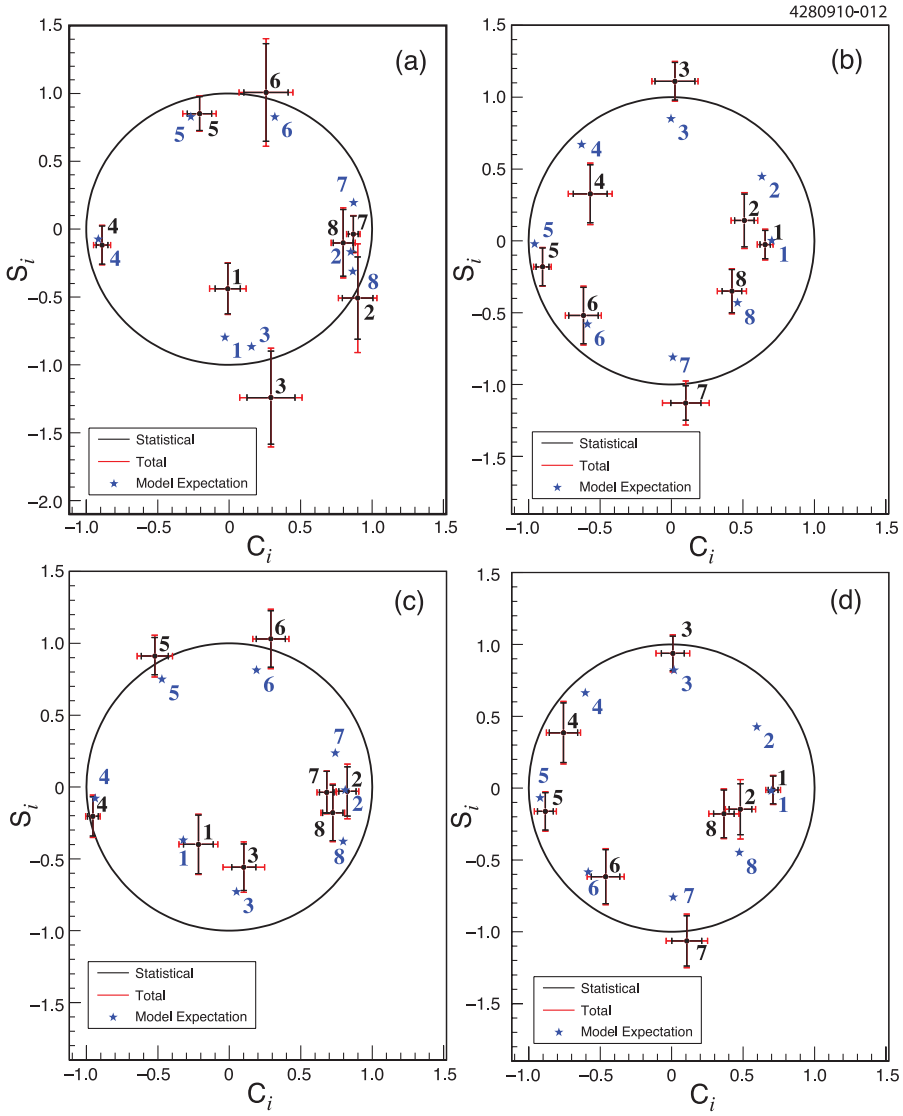

FIG. 14 (color online). Measured values of c_i and s_i for (a) the optimal binning, (b) the equal $\Delta\delta_D$ binning, (c) the modified-optimal binning, and (d) the equal $\Delta\delta_D$ binning based on the Belle model. The expected values calculated from the *BABAR* 2008 model are indicated by the stars. The circle indicates the boundary of the physical region $c_i^2 + s_i^2 = 1$.

and s_i is approximately 1.3°. For the majority of the $K_S^0\pi^+\pi^-$ binnings, these results demonstrate that, with the exception of the optimal binning choice, the uncertainty on γ/ϕ_3 arising from the errors on the measured c_i and s_i parameters is less than that of the assigned model uncertainty in the unbinned analyses [13,14].

For both $\tilde{D}^0 \to K_S^0 K^+ K^-$ and $\tilde{D}^0 \to K_S^0\pi^+\pi^-$, small biases of $\mathcal{O}(1°)$ are observed in the mean fitted values of γ/ϕ_3. This was also observed in Ref. [7], where the origin of the bias is linked to the assumed values in the fit being unphysical, $c_i^2 + s_i^2 > 1$, in some simulated experiments. If the unphysical simulated experiments are removed the bias is not eliminated because of the non-Gaussian nature of the truncated distributions of c_i and s_i. As before it is found that improvements in the precision of the measurements of c_i and s_i would reduce the bias to a negligible level.

We also investigate how the choice of binning for $\tilde{D}^0 \to K_S^0\pi^+\pi^-$ affects the statistical precision on γ/ϕ_3. The optimal and the modified-optimal binnings have been optimized to minimize the statistical uncertainty on γ/ϕ_3 in the absence of background and with the anticipated background at LHCb [16], respectively. The impact of these binnings on B data can be assessed by comparing them to the equal $\Delta\delta_D$ binning derived from the *BABAR* 2008 model using simulated B data samples. We generate simplified MC samples of 5000 $B^\pm \to K^\pm\tilde{D}^0$ signal events which corresponds to the expected yield with 2 fb^{-1} of LHCb data. The statistical uncertainties on γ/ϕ_3 are 8.0° and 7.0° for the equal $\Delta\delta_D$ and optimal binnings, respectively. This demonstrates the advantage in using the optimized binning, and the improvement is consistent with the increase in the Q quantity given in Table I. We also

TABLE XXI. Values of $Q^{(\prime)}$ derived from the measured values of c_i and s_i for the different binnings. The uncertainty is determined by varying c_i and s_i within their errors accounting for correlations.

Binning	$Q^{(\prime)}$
$D^0 \to K^0_S K^+ K^-$	
$\mathcal{N} = 2$ equal $\Delta\delta_D$	$0.88^{+0.14}_{-0.08}$
$\mathcal{N} = 3$ equal $\Delta\delta_D$	$0.82^{+0.15}_{-0.06}$
$\mathcal{N} = 4$ equal $\Delta\delta_D$	$0.90^{+0.21}_{-0.03}$
$D^0 \to K^0_S \pi^+ \pi^-$	
Optimal	$0.93^{+0.12}_{-0.02}$
BABAR 2008 equal $\Delta\delta_D$	$0.81^{+0.05}_{-0.01}$
Modified optimal	$0.95^{+0.10}_{-0.04}$
Belle equal $\Delta\delta_D$	$0.78^{+0.05}_{-0.01}$

generate samples that include background events with yields according to the LHCb background model described in Sec. III B 4. We find the statistical uncertainties on γ/ϕ_3 of 15.0°, 15.4°, and 14.6° for the equal $\Delta\delta_D$, optimal and modified-optimal binning, respectively. This shows that in the presence of background the modified-optimal binning has a smaller statistical uncertainty than the other binnings as expected from the Q' values given in Table I.

As an additional cross check of the sensitivity to γ/ϕ_3 we determine $Q^{(\prime)}$ for the different binnings from the measured values c_i and s_i. The measured values of Q' are given in Table XXI. In all cases the values indicate good sensitivity to γ/ϕ_3 relative to the unbinned method. In addition the values are in reasonable agreement with the predictions presented in Sec. III.

C. *CP* fraction in the region of the ϕ resonance in $D^0 \to K^0_S K^+ K^-$ decays

The *CP*-odd fraction of $D^0 \to K^0_S K^+ K^-$ decays has been estimated using the expression given in Eq. (13). The values of $M^{+}_{(-)i}$ are measured for four different bins defined as having $|\Delta m^2_{K^+K^-}|$ less than 0.006, 0.010, 0.014, and 0.018 GeV$^2/c^4$. Here, $\Delta m^2_{K^+K^-} = m^2_{K^+K^-} - m^2_\phi$, where m_ϕ is the nominal ϕ mass [23]. The different ranges allow the result best suited to the experimental resolution to be used in evaluating any systematic uncertainty related to the *CP* content of the $D^0 \to K^0_S \phi$ decay. The results are given in Table XXII. The systematic uncertainty contains contributions from the migration matrix uncertainties, background parameterizations, and branching fraction uncertainties. The methods for determining the systematic uncertainties are identical to those used for $c_i^{(\prime)}$ and $s_i^{(\prime)}$.

To improve the precision of the measurement we also determine the *CP*-even fraction, $\mathcal{F}_+$, for $D^0 \to K^0_L K^+ K^-$ decays in the same mass-squared intervals. The measurements are given in Table XXII; the significant sources of systematic uncertainty are the same as those for the value of $\mathcal{F}_-$ measured from $D^0 \to K^0_S K^+ K^-$ decays, but are largely uncorrelated. The value of $\mathcal{F}_+$ for $D^0 \to K^0_L K^+ K^-$ decays will be slightly different to $\mathcal{F}_-$ for $D^0 \to K^0_S K^+ K^+$ decays for the same reason that c_i and s_i differ from c_i' and s_i', as discussed in Sec. V. Therefore, we correct the measured value of $\mathcal{F}_+$ before combining it with the measurement of $\mathcal{F}_-$. We define $\Delta\mathcal{F}$ as the value of $\mathcal{F}_+$ for $D^0 \to K^0_L K^+ K^-$ decays minus the value of $\mathcal{F}_-$ for $D^0 \to K^0_S K^+ K^-$ decays predicted by the *BABAR* amplitude model [14]. The value of $\Delta\mathcal{F}$ is given in Table XXII; the uncertainty on $\Delta\mathcal{F}$ is determined in identical fashion to those on Δc_i and Δs_i, as described in Sec. V. We then subtract the value of $\Delta\mathcal{F}$ from the measured value of $\mathcal{F}_+$ for $D^0 \to K^0_L K^+ K^-$ decays and average the result with $\mathcal{F}_-$. The combined values of $\mathcal{F}_-$ are given in Table XXII. The systematic uncertainty on the average value of $\mathcal{F}_-$ has a significant contribution from the error on $\Delta\mathcal{F}$ as well as the other sources already discussed.

The results are consistent with no contamination from *CP*-odd eigenstates in the region of the ϕ resonance for all $m^2_{K^+K^-}$ intervals. The values of $\mathcal{F}_-$ can be greater than one due to the background subtraction resulting in a negative yield. We calculate the lower limit on $\mathcal{F}_-$ at the 90% confidence level (C.L.), by integrating the Gaussian distribution of the average value of $\mathcal{F}_-$ within the physical region $0 \le \mathcal{F}_- \le 1$. The lower limits on $\mathcal{F}_-$ at the 90% C.L. are 0.89, 0.91, 0.76, and 0.77 for $|\Delta m^2_{K^+K^-}|$ less than 0.006, 0.010, 0.014, and 0.018 GeV$^2/c^4$, respectively.

VIII. SUMMARY

Using 818 pb^{-1} of data collected by the CLEO-c detector at the $\psi(3770)$ resonance we have presented measurements of the amplitude-weighted averages of the cosine and sine of

TABLE XXII. Measured values of $\mathcal{F}_-$ ($\mathcal{F}_+$) for $D^0 \to K^0_S K^+ K^-$ ($D^0 \to K^0_L K^+ K^-$) decays with different criteria on $\Delta m^2_{K^+K^-}$. The predicted value of $\Delta\mathcal{F}$ and the average value of $\mathcal{F}_-$ for $D^0 \to K^0_S K^+ K^-$ and $D^0 \to K^0_L K^+ K^-$ are also given. The first uncertainty is statistical and the second is systematic.

Criterion on $\lvert\Delta m^2_{K^+K^-}\rvert$	$D^0 \to K^0_S K^+ K^-$ $\mathcal{F}_-$	$D^0 \to K^0_L K^+ K^-$ $\mathcal{F}_+$	$\Delta\mathcal{F}$	Combined $\mathcal{F}_-$
<0.006 GeV$^2/c^4$	$1.09 \pm 0.09 \pm 0.09$	$0.98 \pm 0.09 \pm 0.02$	-0.02 ± 0.04	$1.03 \pm 0.07 \pm 0.04$
<0.010 GeV$^2/c^4$	$1.13 \pm 0.08 \pm 0.08$	$0.98 \pm 0.07 \pm 0.02$	-0.02 ± 0.04	$1.05 \pm 0.06 \pm 0.04$
<0.014 GeV$^2/c^4$	$0.73 \pm 0.27 \pm 0.04$	$0.90 \pm 0.09 \pm 0.02$	-0.02 ± 0.05	$0.90 \pm 0.10 \pm 0.02$
<0.018 GeV$^2/c^4$	$0.75 \pm 0.22 \pm 0.04$	$0.90 \pm 0.08 \pm 0.02$	-0.03 ± 0.06	$0.90 \pm 0.09 \pm 0.02$

the strong phase differences beween D^0 and $\bar{D}^0 \to K^0_{S,L}h^+h^-$ ($h = \pi, K$) decays in bins of Dalitz space, $c_i^{(\prime)}$ and $s_i^{(\prime)}$. These results are necessary input for performing model-independent measurements of the CKM-angle γ/ϕ_3 [5,19] and can also be used in model-independent determinations of the charm-mixing parameters [9].

The results for $D^0 \to K^0_S\pi^+\pi^-$ are an update to those of our earlier publication [7]. The measurements presented here benefit from an improved analysis procedure and bin choices informed by an amplitude model developed by the *BABAR* Collaboration [12] which provides a better description of Dalitz space than was previously available. We have given results for bin choices made with an equal division in strong-phase difference ('equal $\Delta\delta_D$') and for a division which optimizes the foreseen precision on γ/ϕ_3 in a low background environment (''optimal''), as expected at an e^+e^- experiment, and for one (''modified optimal'') which gives the best result under the background conditions anticipated at a hadron-collider experiment such as LHCb. Results have also been presented for an equal $\Delta\delta_D$ binning based on an amplitude model devised by the Belle Collaboration [13]. We estimate the uncertainty on γ/ϕ_3 to be between 1.7° and 3.9°, depending on the binning, due to the uncertainties on the measured values of c_i and s_i. In most cases, this uncertainty is smaller than that due to the $D^0 \to K^0_S\pi^+\pi^-$ amplitude model in the most recent analyses [13,14].

The results for $D^0 \to K^0_SK^+K^-$ are the first measurements of $c_i^{(\prime)}$ and $s_i^{(\prime)}$ for this decay. They have been given for equal $\Delta\delta_D$ divisions of Dalitz space based on the amplitude model found in Ref. [14] for each half of the Dalitz plot divided into two, three and four bins. The uncertainty on γ/ϕ_3 from the error on c_i and s_i parameters is between 3.2° and 3.9° depending on the binnings; these uncertainties are comparable to those related to the amplitude model in the unbinned analysis [14].

We test the compatibility of the measured values of c_i and s_i with those predicted by the amplitude models derived from flavor-tagged samples of $D^0 \to K^0_Sh^+h^-$ decays. The agreement is reasonable in all cases, indicating that there are no large errors in the phase measurements provided by these models.

In addition, we determine the CP-odd fraction, $\mathcal{F}_-$, for $D^0 \to K^0_SK^+K^-$ decays in the region of the ϕ resonance. The results are given in different ranges of invariant-mass squared about the ϕ resonance. In all intervals considered $\mathcal{F}_-$ is greater than 0.76 at 90% C.L. This result will better constrain systematic uncertainties related to the CP-even content when $D^0 \to K^0_S\phi$ is used as a CP-odd eigenstate in an analysis.

ACKNOWLEDGMENTS

We gratefully acknowledge the effort of the CESR staff in providing us with excellent luminosity and running conditions. D. Cronin-Hennessy thanks the A. P. Sloan Foundation. This work was supported by the National Science Foundation, the U.S. Department of Energy, the Natural Sciences and Engineering Research Council of Canada, and the U.K. Science and Technology Facilities Council.

[1] N. Cabibbo, Phys. Rev. Lett. **10**, 531 (1963); M. Kobayashi and T. Maskawa, Prog. Theor. Phys. **49**, 652 (1973).
[2] A. Höcker *et al.* (CKMfitter Group), Eur. Phys. J. C **21**, 225 (2001); J. Charles *et al.* (CKMfitter Group), Eur. Phys. J. C **41**, 1 (2005), and updates at http://ckmfitter.in2p3.fr/.
[3] M. Ciuchini *et al.*, J. High Energy Phys. 07 (2001) 013; M. Bona *et al.* (UTFit Collaboration), J. High Energy Phys. 10 (2006) 081, and updates at http://www.utfit.org/.
[4] M. Gronau and D. Wyler, Phys. Lett. B **265**, 172 (1991); M. Gronau and D. London, Phys. Lett. B **253**, 483 (1991).
[5] A. Giri, Y. Grossman, A. Soffer, and J. Zupan, Phys. Rev. D **68**, 054018 (2003).
[6] A. Bondar, in *Proceedings of BINP Special Analysis Meeting on Dalitz Analysis, 2002* (unpublished).
[7] R. A. Briere *et al.* (CLEO Collaboration), Phys. Rev. D **80**, 032002 (2009).
[8] Y. Grossman, A. Soffer, and J. Zupan, Phys. Rev. D **72**, 031501(R) (2005).
[9] A. Bondar, A. Poluektov, and V. Vorobiev, Phys. Rev. D **82**, 034033 (2010).
[10] A. Poluektov *et al.* (Belle Collaboration), Phys. Rev. D **70**, 072003 (2004); **73**, 112009 (2006).
[11] B. Aubert *et al.* (*BABAR* Collaboration), Phys. Rev. Lett. **95**, 121802 (2005).
[12] B. Aubert *et al.* (*BABAR* Collaboration), Phys. Rev. D **78**, 034023 (2008).
[13] A. Poluektov *et al.* (Belle Collaboration), Phys. Rev. D **81**, 112002 (2010).
[14] P. del Amo Sanchez *et al.* (*BABAR* Collaboration), Phys. Rev. Lett. **105**, 121801 (2010).
[15] J. Libby, CERN, Report No. CERN-LHCb-2007-141, 2007.
[16] V. Gibson, C. Lazzeroni, and Y.-Y. Li, CERN, Report No. CERN-LHCb-2008-028, 2008.
[17] T. Aushev *et al.*, KEK-Report 2009-12, 2010.
[18] M. Bona *et al.*, Report Nos. SLAC-R-856, INFN-AE-07-02, LAL-07-15, 2007.
[19] A. Bondar and A. Poluektov, Eur. Phys. J. C **47**, 347 (2006); **55**, 51 (2008).
[20] D. M. Asner *et al.* (CLEO Collaboration), Phys. Rev. D **72**, 012001 (2005); L. M. Zhang *et al.* (Belle Collaboration),

Phys. Rev. Lett. **99**, 131803 (2007); A. Zupanc *et al.* (Belle Collaboration), Phys. Rev. D **80**, 052006 (2009); P. del Amo Sanchez *et al.* (*BABAR* Collaboration), Phys. Rev. Lett. **105**, 081803 (2010).

[21] N. Lowrey *et al.* (CLEO Collaboration), Phys. Rev. D **80**, 031105 (2009).

[22] K. Abe *et al.* (Belle Collaboration), Phys. Rev. D **73**, 051106 (2006).

[23] K. Nakamura *et al.* (Particle Data Group), J. Phys. G **37**, 075021 (2010).

[24] F. Martinez-Vidal and N. Lopes-March (private communication).

[25] S. M. Flatte, Phys. Lett. **63B**, 224 (1976).

[26] I. J. R. Aitchison, Nucl. Phys. **A189**, 417 (1972).

[27] D. Aston *et al.* (LASS Collaboration), Nucl. Phys. **B296**, 493 (1988).

[28] A. Poluektov (private communication).

[29] Y. Kubota *et al.* (CLEO Collaboration), Nucl. Instrum. Methods Phys. Res., Sect. A **320**, 66 (1992); D. Peterson *et al.*, Nucl. Instrum. Methods Phys. Res., Sect. A **478**, 142 (2002); M. Artuso *et al.*, Nucl. Instrum. Methods Phys. Res., Sect. A **554**, 147 (2005).

[30] D. Lange *et al.*, Nucl. Instrum. Methods Phys. Res., Sect. A **462**, 152 (2001).

[31] R. Brun *et al.*, GEANT 3.21, CERN Program Library Long Writeup W5013 (unpublished).

[32] S. Dobbs *et al.* (CLEO Collaboration), Phys. Rev. D **76**, 112001 (2007).

[33] D. M. Asner *et al.* (CLEO Collaboration), Phys. Rev. D **78**, 012001 (2008).

[34] Q. He *et al.* (CLEO Collaboration), Phys. Rev. Lett. **100**, 091801 (2008).

[35] D. Atwood and A. Soni, Phys. Rev. D **68**, 033003 (2003).

[36] E. Barberio *et al.* (Heavy Flavor Averaging Group), arXiv:0808.1297, and updates at http://www.slac.stanford.edu/xorg/hfag/.

[37] X. C. Tian *et al.* (Belle Collaboration), Phys. Rev. Lett. **95**, 231801 (2005).

[38] I. I. Bigi and H. Yamamoto, Phys. Lett. B **349**, 363 (1995).

[39] H. Muramatsu *et al.* (CLEO Collaboration), Phys. Rev. Lett. **89**, 251802 (2002).

[40] See supplementary material at http://link.aps.org/supplemental/10.1103/PhysRevD.82.112006 for the bitmaps of the different binnings and the statistical and systematic correlation matrices among parameters.